

**Monitoring the condition of unpaved roads
with remote sensing and other technology**

Final Report for US DOT DTPH56-06-BAA-0002

Principal Investigator: Dr. Chunsun Zhang

Geographic Information Science Center of Excellence

South Dakota State University

Foreword

This project investigates remote sensing technology for monitoring condition of unpaved roads. The unpaved roads are usually low-volume roads serving remote areas and agricultural business and linking agricultural communities to nearby towns and markets. Although more than half of all US roads are unpaved, assessment of unpaved road condition has been rarely addressed in transportation research. Current approach for unpaved road condition data collection is time-consuming and labor extensive. The construction and maintenance of unpaved roads is generally performed by local townships and county governments. Due to limited funding, local officials typically rely on visual inspection, intuition and occasional spot measurements in their assessments. Thus, these unpaved roads are usually inadequately inspected and assessed. Yet the importance of timely identification and rectification of road deformation cannot be overstated.

The primary thrust of this project is to develop an efficient and cost-effective system and methods for the collection of unpaved road condition data in support of the road management needs of transportation agencies and local government. We explore the use of Unmanned Aerial Vehicle (UAV) as a road data collection platform, and develop efficient methods and systems to process UAV images and identify and quantify unpaved road surface condition parameters.

The UAV-based remote sensing system consists of a low cost model helicopter equipped with a GPS/IMU and a digital camera. An autonomous flight control system is employed to control the flight mission of the helicopter with a ground control system. We have developed a set of image processing algorithms for camera calibration, sensor orientation, digital 3D road surface model and orthoimage generation, and measurement for road surface distress. The developed system has been tested over a number of rural roads with various surface conditions. Road images has been acquired and processed, and the size and dimension of surface distresses are measured efficiently with sufficient accuracy. The difference of one centimeter between image-based measurement and precise ground survey demonstrates the capability of the developed system and indicates the strong potential for practice in future. The developed system is faster, safer and more consistent than manual surveys. The acquired road imagery, together with the derived 3D road images and condition measurements can be directly integrated into rural road management system, thereby, allowing more efficient management of rural road networks.

Acknowledgement

This research is supported by US Department of Transportation under grant DTOS59-07-H-0007, and performed at Geographic Information Science Center of Excellence (GIScCE), South Dakota State University.

The team members include Dr Chunsun Zhang, Dr Ahmed Elaksher, Dr Binxuan Guo, former GIScCE graduate students Ms Tsolmongerel Papilloud, Ms Sabina Shahnaz at GIScCE, Mr Dave Huft of South Dakota State Department of Transportation and Mr Ken Skorseth of South Dakota Local Transportation Assistance Program. Team members Ms Mary O'Neill and Mr Kevin Dalsted of SDSU Engineering Resource Center participated in the project meetings and provided valuable suggestions. We acknowledge the field work of SDSU graduate students Mr Pradip Maharhan, Mr. Ali Aijaz and Mr K C Pramod.

We thank Mr Caesar Singh, the program manager of USDOT for his strong support, valuable advices, and many discussions.

GIScCE provided matching funds for this research. We acknowledge the support of Dr Matthew Hansen in carrying out this project.

This project also benefits from the discussions and comments of the advisory committee composed by experts from the Central Federal Lands Highway Division of Federal Highway Administration, South Dakota Department of Transportation, Northern Plains Tribal Technical Assistance Program, SD Assn. of Towns & Townships, Federal Highway Administration (SD Division), and Brookings County Highway Department.

We thank Brookings Highway Department, Brookings local road maintenance teams for their discussions and suggestions in test site selection and data collection.

Table of Contents

Chapter 1. Introduction.....	7
Chapter 2. Unpaved Road and Road Condition Assessment.....	9
2.1 Unpaved Roads and Road Condition.....	9
2.2 Approaches to Road Condition Assessment.....	11
Chapter 3. Conceptual Approach to Road Condition Evaluation.....	15
Chapter 4. Overview of the UAV System.....	18
Chapter 5. Algorithms for Image-based Measurement of Surface Distress.....	20
5.1 Camera Calibration.....	21
5.2 Image Orientation.....	21
5.3 Feature Point Extraction and Matching.....	23
5.4 Relative Orientation.....	25
5.5 Bundle Adjustment Free Network.....	26
5.6 3D Reconstruction for Measurement of Surface Distresses.....	28
Chapter 6. Experiment Tests.....	32
6.1 Test Site Description.....	32
6.2 Image Acquisition.....	34
6.3 Image Analysis for 3D Reconstruction for Measurement of Surface Distresses	37
6.4 Accuracy Analysis.....	44
Chapter 7. Discussions.....	45
Chapter 8. Conclusions and Recommendations.....	47
Reference.....	49

List of Figures

Figure 1. Unpaved roads and road condition.

Figure 2. Examples of ground measurement of surface distress.

Figure 3. UAV-acquired road imagery.

Figure 4. Conceptual Approach of UAV-based remote sensing of unpaved road condition.

Figure 5. System overview.

Figure 6. UAV-based imaging system.

Figure 7. Graphic user interface of weGCS on ground control station.

Figure 8. Principle of 3D reconstruction from overlapped images.

Figure. 9. Flowchart of data processing of the developed road condition collection system.

Figure 10. Outline of image orientation approach.

Figure 11. Extracted feature points (in red) by the SIFT method from a road image.

Figure 12. Results of matching two different image pairs in the along-track direction (top) and in the across-track direction (bottom).

Figure 13. Imaging process and 3D reconstruction from images.

Figure 14. Determination of Z coordinate of grid point A (X_A, Y_A) with initial Z value Z_0 . Z_A is in the range ($Z_0 - \text{deltZ}, Z_0 + \text{deltZ}$).

Figure 15. Test site.

Figure 16. Examples of road image in the test site.

Figure 17. Example of road images acquired by UAV over a road segment.

Figure 18. UAV acquired image allows for evaluation of culvert.

Figure 19. Road image acquired by UAV showing severe ruts. Note the marks are designed for ground measurements and for relating ground measurements with image measurements.

Figure 20. 3D view of automatic image block formation and image orientation.

Figure 21. Residual of bundle adjustment on the image block in Figure 10.

Figure 22. 3D reconstruction of rut.

Figure 23. 3D reconstruction of pothole from UAV-acquired imagery.

Figure 24. 3D reconstruction of pothole from UAV-acquired imagery.

Figure 25. Measurement of the size of ruts and potholes.

Figure 26. Reproduce of 3D image of road with large and severe distress from UAV-acquired imagery.

Chapter 1 Introduction

More than half of all US roads (and more than 90% of roads globally) are unpaved (Skorseth and Selim, 2000). They serve remote areas and a few vehicles. On the other hand, gravel roads serve agriculture, logging and recreational areas with fairly high volume of traffic. Unpaved roads are also found in many urban areas. In the Great Plains, these unpaved roads are typically low-volume roads linking small agricultural communities to nearby towns and markets. These roads tend to experience marked seasonal variations in traffic volumes with significantly higher flows occurring around harvest time each year. If periods of wet weather and high traffic volumes coincide, damage to unpaved roads can be very severe. Such roads are also susceptible to damage because of the kind of vehicles that traverse them. Heavy farm machinery and trucks laden with farm produce can do more damage to a road than a series of smaller vehicles of equal net mass. Consequently, the annual average daily traffic numbers used to classify many unpaved roads as low-volume roads often do not tell the full story of the loading on the road.

The construction and maintenance of unpaved roads is generally performed by local townships and county governments. Because of the small funding base of local government, the human and financial resources available for maintaining roads are often inadequate. Local infrastructure engineers and supervisors must therefore optimize their resources when monitoring road conditions and scheduling maintenance activities. As a precursor to scheduling maintenance activities, local transportation departments must conduct field surveys to identify problem areas and schedule maintenance activities. In South Dakota, for example, a team of local road supervisors will typically conduct one field survey each year to determine which sections of roads need repair. Given that a county may have more than 500 miles of road, it is unlikely that every section of road within a county will be adequately inspected during a single trip. Also, while state and federal transportation departments often have vehicle-mounted roughometers and other devices to assess road surface conditions, local officials typically rely on visual inspection, intuition and occasional spot measurements in their assessments. Yet the importance of timely identification and rectification of road deformation through loss of crown or damage to the road base cannot be overstated.

This research, supported by Research and Innovative Technology Administration (RITA), the U.S. Department of Transportation (USDOT Remote Sensing Cooperative Agreement #DTOS59-07-H-0007), explores the potential for applying remote sensing technology to monitoring the condition of unpaved roads. It aims to develop a simple yet robust, operational, cost-effective system for maintaining statewide information on the condition of unpaved roads without having to rely on in-situ surveys. The primary thrust of this project is to develop efficient and cost-effective methods for the collection of road condition data

We explore the use of an Unmanned Aerial Vehicle (UAV) as a road data collection platform, and develop efficient methods and systems to process UAV images and identify and quantify road condition parameters such as rutting, potholes, and road surface roughness. The research

necessary includes development of methods for UAV sensor calibration and orientation, and accurate geopositioning, and development of efficient image processing algorithms for automated 3D reconstruction of road surface and measurement of surface distresses.

This report is organized in following. After this introduction, we review unpaved road condition and current experiences of condition evaluation in Chapter 2. Chapter 3 presents our proposed strategy. The designed UAV-based remote sensing system for road data collection is shown in Chapter 4. We then discuss in detail the developed image analysis technologies to process the UAV-acquired road images in Chapter 5. The whole system has been tested over a number of roads and the measurements obtained were compared with ground survey conducted simultaneously during image acquisition. The tests and test results are reported in Chapter 6. Based on the test results, discussions were given in Chapter 7. Finally, conclusions are drawn, and further researches are recommended in Chapter 8.

Chapter 2 Unpaved Roads and Road Condition Assessment

2.1 Unpaved roads and road condition

Unpaved roads demonstrate a variety of conditions. A newly constructed or well maintained road should have excellent surface condition and provides smooth and safety traffic. However, the unpaved roads can be deteriorated very quickly due to traffic, weather, bad habit of driving etc. Excessive use of roads and heavy traffic during planting in spring and summer and harvest in fall damage roads more quickly and frequently. Significant rainfall washes away gravel from surface, resulting in loss of adequate crown. Water trapped on roads cause potholes. Heavy traffic, bad driving habit such as excessive acceleration tend to damage roads and develop ruts, aggregates (washboards). Disturbances to unpaved road surfaces and ditches, and poor road surface drainage always results in deterioration of the road surface. In northern states, unpaved roads are also susceptible to accelerated damage during the spring thaw period. The uneven thaw pattern results in water trapped between different layers of road. Typical distresses during this thaw state include severe ruts and large potholes. These damaged roads, if not promptly repaired, tend to be degraded more quickly with severe weather and traffic. In general, distresses on roads create difficulty to local community in day-to-day commute, transport of goods, and seasonal farming practice. In addition, the deteriorated roads pose a major challenge in traffic safety. Some typical unpaved road conditions are shown below in Figure 1.





Figure 1. Unpaved roads and road condition. The images of top row show two roads in good condition. The roads shown in the images of the two middle rows demonstrate significant surface distresses, such as potholes, loss of crown, resulting water trapped on surface after rainfall which in turn further deteriorating roads in they are not properly repaired. The last row gives examples of roads with corrugation effects and severe rutting.

2.2 Previous work on road condition assessment

Road management system is important to state DOTs and local transportation authorities. An important component of such management system is surface condition survey and rating procedures. The predominant method in conducting road condition survey and analysis is still largely based on extensive field observation by experts. This method is slow, expensive, prone to error and poses safety problems.

Due to the nature of gravel roads and their variability, evaluation and rating gravel roads requires a different perspective than similar evaluations of asphalt or concrete pavements. Unpaved road condition is related to several factors, including structural integrity, structural capacity, roughness and rate of deterioration (Eaton and Beaucham, 1992). Direct measurement of all of these factors requires expensive equipment and highly trained personnel. However, these factors can be assessed by observing and measuring the distress of the surface. Commonly used evaluation approaches are based on Gravel PASER Manual (Walker et al., 2002) from Wisconsin Transportation Information Center and Unsurfaced Road Maintenance Management (Eaton and Beaucham, 1992) from US Army Corps of Engineers. The two documents have identified various distresses of unpaved roads and suggest measurement methods for each individual type of distress. Data obtained from these procedures are the primary basis for determining maintenance and repair requirements and priorities.

Gravel PASER Manual (2002) suggests focus on major factors as well as detailed surface conditions. These include Crown, Drainage, Gravel layer, Surface deformation and Surface defects. Similarly, In Unsurfaced Road Maintenance Management, road condition is determined through Unsurfaced Road Condition Index (URCI), a numerical indicator based on a scale of 0 to 100. URCI indicates the roads integrity and surface operational condition. URCI is determined by measuring seven surface distresses, including improper cross section, inadequate road side drainage, corrugations, dust, potholes, ruts, loose aggregate. The detailed definition of severity of each distress and approach to the measurements are given in the both documents. State DOTs also provide guidelines of identification of distress and determination of severity.

Following the documents, condition survey of unpaved roads is conducted by ground measurements. Usually, a two-person team is required. While the equipments needed to do a survey are simple and just a hand odometer used to measure distress lengths and areas, a straight edge, and a ruler to measure the depths of potholes, ruts, or loose aggregate, however, the measurement can be very time consuming and labor extensive. Figure 3 shows examples of ground measurement of ruts, pothole and cross section slope. Typically, it takes around 20~40 minutes for measurement on a single spot. The passing traffic and extreme weather condition can further stress the difficulty of the work, requiring even longer time for each measurement.



Measurement of ruts depth



Measurement of cross section slope



Measurement of pothole depth

Figure 2. Examples of ground measurement of surface distress.

Due to the high cost and difficulty of ground measurement, such survey is not affordable to most of the local road management authorities, and is conducted only occasionally. Local transportation management agencies largely rely on simple windshield inspection, or even no survey at all in many regions. The maintenances of the damaged roads are then performed based on the local authority discussions or even complaints of local residences.

While little attention has been paid on the advancement of unpaved road evaluation approach, research of pavement assessment has been very active in transportation agencies and research community. The technologies developed in pavement evaluation may provide some hints and incentives. Some may be adaptable to unpaved road maintenance with modifications and

improvements. Recent efforts on pavement condition assessment are to develop pavement survey vehicle coupled with sensor technologies and data-processing onboard (Wang, 2000; Gunaratne et al., 2003; Sokolic et al., 2004;). Some systems have been used in highway agencies (Kenneth, 2004). However, no similar technology or system exists for unpaved roads. Nevertheless, data collection using a moving vehicle still remains an expensive and troublesome survey, while cost and safety considerations require that it be done at regular intervals. Static/dynamic sensors distributed over road sections are also used to record the pavement response to traffic loading and environment data which are used to evaluate the effects of heavy vehicles on pavement, the effects of seasonal changes in paving materials (<http://www.mrr.dot.state.mn.us/research/mnresearch.asp>).

More recently, commercial remote sensing technologies and methods are introduced in transportation practices. Remote sensing imagery, with its recently enhanced spatial, spectral and temporal resolution, provides more details of the earth surface and allows for accurate and reliable detection and characterization of the terrain and the patterns of earth with higher accuracy (Fraser et al., 2006; Poon et al., 2005; Poon et al., 2006), thus also benefit the transportation applications. For example, aerial images and photogrammetry techniques have been the principal technology for corridor planning and development. Accurate 3D road network can be automatically extracted from airborne and spaceborne imagery (Zhang, 2003; Baltasvias et al., 2004; Baltasvias and Zhang, 2005). Even higher resolution satellite imaging systems, such as Worldview-1, Worldview-2 from DigitalGlobe, are currently available, providing multispectral imagery with 41cm resolution (<http://www.digitalglobe.com/>). In addition, LIDAR as a new technology is gaining rapid adoption by many state transportation agencies. Recent research progress and achievements on remote sensing in transportation applications have been reported in NCRST (2000, 2003a, 2003b, 2004). In pavement assessment, a study has been conducted by the University of California Santa Barbara in joint collaboration with Iowa State University to find a correlation between spectral reflectance and physical characteristics such as rutting and cracking (NCRST, 2003a). The results show it is possible to describe general pavement age and specific surface defects such as raveling, and to estimate their spatial characteristics. Due to limited spatial resolution (4m) of the sensor used (NASA/JPL AVIRIS), they found other important pavement quality parameters such as rutting and cracking are undetectable. A further effort was performed using sub-meter (50cm) hyperspectral remote sensing data (Herold et al., 2004). They use image ratios and the spatial variance measures and relate them with road condition parameters such as Pavement Condition Index (PCI). With the increased spatial resolution, the image ratios show correlation with PCI, and variance correlated with an index describing structural road damages, demonstrating the potential of remote sensing in road condition mapping. While the results of this research are promising, however, problems still remain. The main drawback of this method is that it relies only on spectral information, thus the results are not always accurate. Especially on older roads which might be subject to maintenance, the results usually tend to uncertain. This suggests further research to develop a more efficient road mapping strategy. First, the road image should contain sufficient detail. In

addition, sophisticated methods should be developed to extract various road features and fuse them to derive robust and reliable road condition parameters to meet the operational use in transportation agencies.

Chapter 3 Conceptual Approach of UAV-based Road Condition Evaluation

Motivated by rapidly advancement of remote sensing and information technology, we explore the use of UAV based remote sensing and image processing technologies for the assessment of unpaved roads.

As discussed in Chapter 2, high resolution image data is essential in order to efficiently detect and measure features on unpaved roads for road condition monitoring. Aerial imagery can be a choice, but the limited maneuverability of the platform to acquire the image data and the associated high costs are shortcomings. In contrast, UAVs are highly flexible. UAVs can be programmed off-line and controlled in real time to navigate and to collect transportation data using a variety of multiple and interchangeable imaging devices and other sensors (NCRST, 2003c). In addition, UAVs are able to operate rather close to the object, acquiring image with resolution as fine as a few centimeters (Eisenbeiss et al., 2005; UVS International, 2006; Zhang, 2009; Zhang and Elaksher, 2009). Examples of UAV-acquired high resolution images are given in Figure 3. Figure 3(a) shows a pavement image captured with 3cm spatial resolution. Such image presents clearly pavement surface with fine structures in sufficient details which allows for identification and extraction of road condition parameters. Figure 3(b) is an unpaved road imagery collected by our UAV. Even tire prints are clearly visible, demonstrating the capability and potential of such image for identification and measurement of the ruts. Furthermore, the UAVs today have many advantages over satellites and manned aircraft, such as collecting image data at a lower cost, faster and more safely. For this reasons, UAVs have been employed in various research and applications, including precision agriculture/forestry (Herwitz, 2002; Xiang and Tian, 2007), surveillance (Kontitsis et al., 2004; Ameri et al., 2008), traffic management (Srinivasan et al., 2004; Coifman et al., 2004), and generation of geospatial products (Zhou and Li, 2006; Eisenbeiss, 2006).

Our developed UAV-based remote sensing system acquires road imagery with high resolution from an UAV helicopter, and assesses roads based on the condition parameters derived through the development of sophisticated algorithms for image processing and analysis. In contrast to convention ground survey, this new approach performs distress measurement from UAV acquired imagery, therefore, improving the evaluation accuracy and reliability. This approach is faster, safer, and more consistent. In addition, the acquired imagery and developed algorithms may also be useful for the extraction and measurement of other road properties, such as road way width, curvatures, etc. which are also important components in road way management.

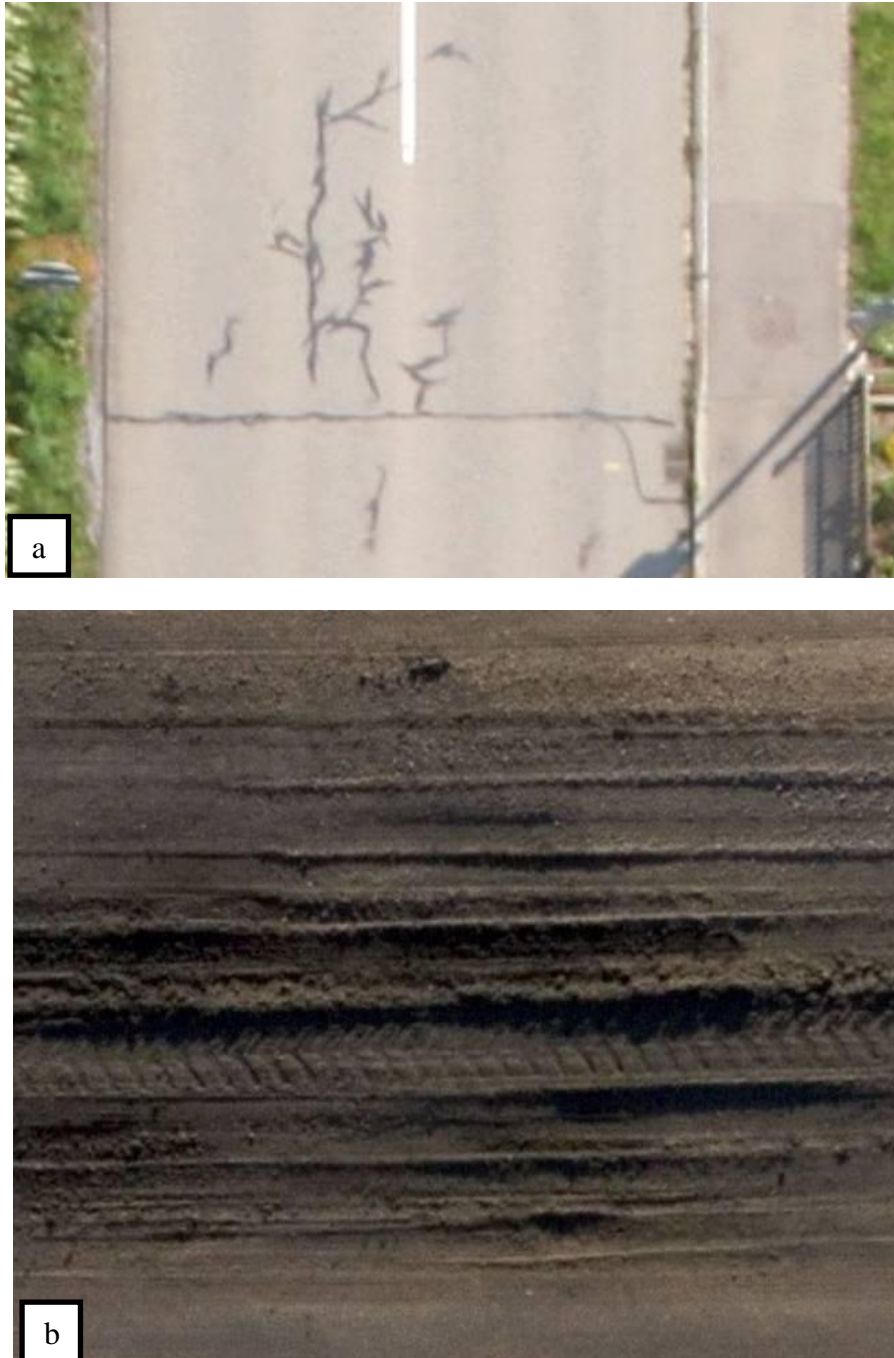


Figure 3. UAV-acquired road imagery. Top: a portion of pavement image with 3cm resolution. Bottom: a portion of image with of 5mm resolution acquired by our UAV over a ruts area.

Our work focus on acquiring imagery using a UAV and extracting information from the image data. The conceptual approach is presented in Figure 4. In addition to the operation of UAV for road image collection, the research includes development of the processing methods for accurate positioning and measurement from imagery, automated extraction of accurate digital surface model, and generation of high resolution orthoimages, and measurement of distresses. The

measured parameters facilitate derivation of information about road quality to enable advanced warning of road deterioration. System tests are conducted, and the performance of system is compared with detailed ground survey to determine the measurement quality.

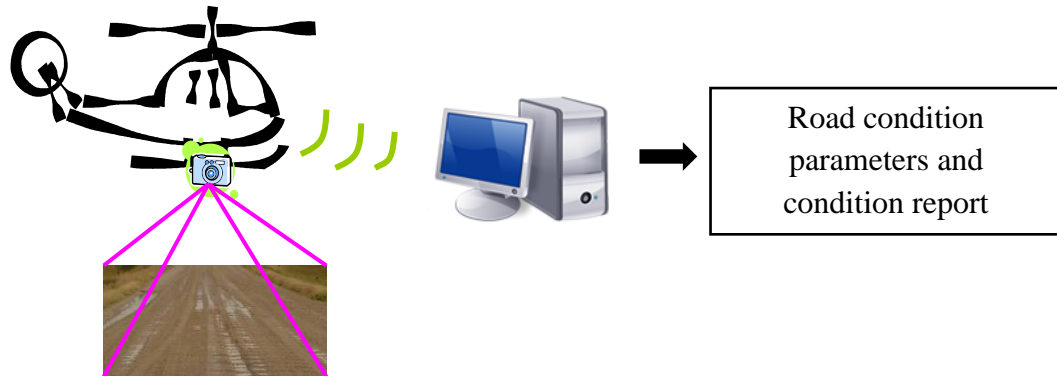


Figure 4. Conceptual approach of UAV-based remote sensing of unpaved road condition.

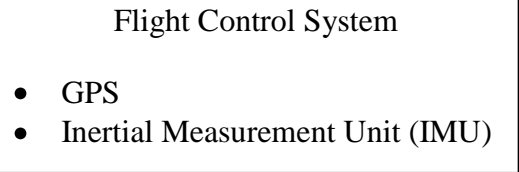
Chapter 4 Overview of the UAV system

The UAV-based imaging system for unpaved road image acquisition consists of a UAV helicopter, digital camera, on-board flight control system and ground control station (GCS). The system overview is shown in Figure 5.

UAV Wolverine
Electric
Helicopter



+



+



+



Canon XTi RGB Camera

Figure 5. System overview.

The helicopter (Figure 6) features an electric engine. It has a payload of 15lb, and is capable of flying around 25 minutes with fully charged battery. This mini UAV can reach 200m above the ground and travel at a maximum speed of 10m per second.



Figure 6. UAV-based imaging system.

The flight control system includes a GPS/INS and an on-board computer which fuses the GPS and INS observations in real time to navigate the helicopter. Thus, it supports both assisted mode

for speed commands through a joystick and mission mode for pre-programmed flight trajectory tracking.

The weGCS software (Figure 7) from weControl Inc. is installed on the GCS computer. The software features an interface for mission plan allowing for setting of mission parameters. A raster map can be loaded and displayed on the graphic user interface for operator to interactively define flight path and waypoints, set flight height and travel speed. Moreover, the GCS can determine the exposure stations pre-launch based on the camera view angle and the specified image overlap size. During mission, the GCS can communicate with the on-board flight control system to automatically trigger the camera at the preset positions and acquire imagery. This functionality is particularly useful for 3D mapping where imagery with sufficient overlap is necessary. The camera can also be triggered manually by an operator. Currently, a Canon EOS Digital Rebel XTi digital camera has been used in our project. The camera has an approximate focal length of 50mm, a 10.1Mpixel resolution (3888x2592 pixels), and a pixel size of 5.7 μ m.

During mission, the GCS also displays in real time the flight data such as speed, attitude, auto-pilot functionality, and other system features including status indicators of serial data-link connection between GCS and on-board flight control, GPS signal, RC (Remote Control) radio connections which are important to mission safety. This information allows for monitoring of the dynamics of the UAV and helps operator in making right decision in case of emergency.

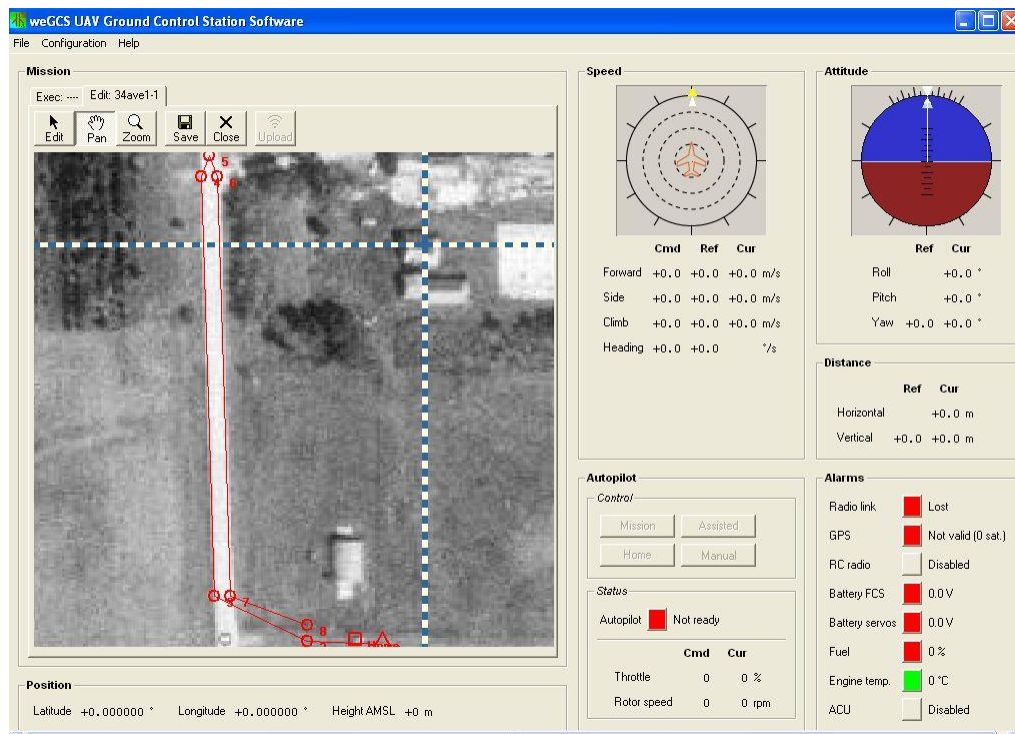


Figure 7. Graphic user interface of weGCS on ground control station.

Chapter 5 Algorithms for Image-based Measurement of Surface Distress

This Chapter presents the developed image analysis algorithms for measurement of surface distress on unpaved roads from UAV-acquired imagery. One of the key developments in this research is reconstruction of 3D road surface from imagery. This is contrast to other image-based approaches to road assessment such as surveying vehicles used in pavement evaluation which measure distress only in 2D. Measurements from 2D image along only provide planimetric data. The inherent third dimension of the observed objects is not obtainable. Such measurements do not allow for full description of road distresses, and thus are inadequate in assessment of distress severity. Indeed, the third dimension data is the key component in road condition evaluation. For instance, the depth of potholes, ruts is obtainable only when the 3D road information is available. Other important road geometric properties, such as road slope, cross section geometry can be derived from 3D data. In addition, 3D information also plays an important role in automated detection of road distresses.

In our research, the 3D data is achieved from overlapped imagery acquired from UAV and by the developed sophisticated image analysis algorithms using digital photogrammetric technologies. Usually, 3D is impossible from single images because information of the third dimension is lost during imaging process. However, from stereo or multiple overlapped images, the third dimension data can be recovered by reversing imaging process. Figure 8 show the principle of imaging process and 3D reconstruction from images. Assume a road point A is captured at a_1 , a_2 and a_3 in images 1, 2 and 3 respectively from perspectives O_1 , O_2 , O_3 . By reversing the imaging process, point A can be reconstructed three-dimensionally by intersecting image rays O_1a_1 , O_2a_2 , and O_3a_3 .

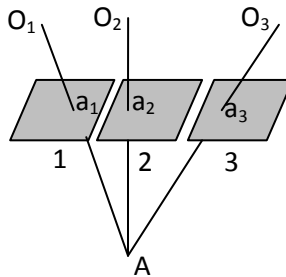


Figure 8. Principle of 3D reconstruction from overlapped images. Ground point A is captured at a_1 , a_2 and a_3 in images 1, 2 and 3 respectively from perspectives O_1 , O_2 , O_3 . Point A can be reconstructed by the intersection of image rays of O_1a_1 , O_2a_2 , and O_3a_3 .

The pre-requisites for precise determination of a ground point are the sensor characteristics and the location and orientation of the image perspective centers. Thus, our system necessarily consists of three main steps: 1) camera calibration, 2) image orientation, 3) 3D reconstruction of surface distresses and distress measurement. The flowchart of image analysis is presented in Figure 9. The input to the system is road images acquired from UVA over road segments. The

system then determines the precise orientation of the images fully automatically. The determined orientation parameters allows for computation of 3D location of each road point from the road images. Furthermore, these parameters are necessary in 3D reconstruction of surface distresses involving multiple image matching for 3D surface model generation and ortho-image generation. The distress areas can be identified either manually by an operator or automatically by computer. In current implementation, they are specified manually on images by simple mouse click. The generated surface model and 3D road images are used for measurement of surface distresses.

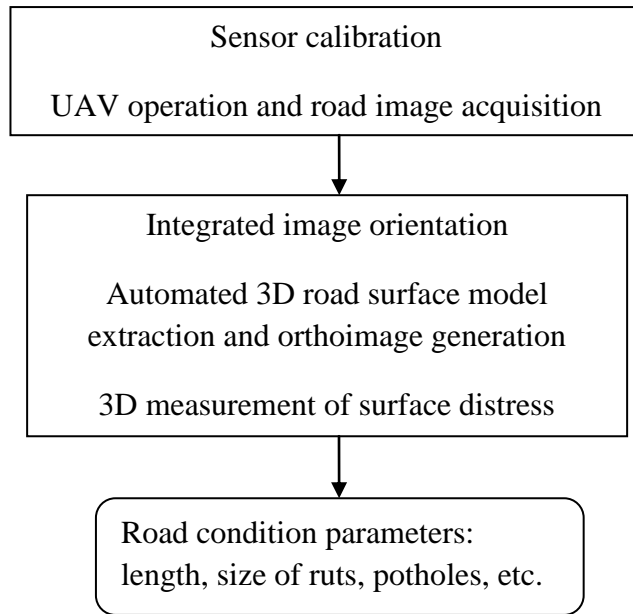


Figure. 9. Flowchart of data processing of the developed road condition collection system.

5.1 Camera Calibration

Camera calibration is necessary for extracting accurate 3D information from images. This topic has been extensively researched in computer vision and photogrammetry (Fraser, 1997; Zhang, 2000; Hartley and Zisserman, 2000; Gruen and Beyer, 2001). The aim of camera calibration is to determine the inner orientation parameters. Several commercial software and open source algorithms for camera calibration are available in the market and the literature. In this research, the camera characteristics are determined via iWitness software (Cronk et al., 2006). The advantage of this software is that it does not request special calibration field with precisely measured 3D points. Instead, color-coded targets are used. During calibration, the color-coded targets can be randomly distributed on the floor or wall and several images are recorded for the scene. Afterwards, the calibration is performed automatically, delivering the calibrated focal length, the principle point coordinates and the distortion parameters. The process is easy to operate and particularly suitable for projects with consumer-grade non-metric cameras that request frequent field calibration.

5.2 Image Orientation

After acquisition of imagery in a UAV flight mission, the imagery should be accurately orientated before 3D mapping and image-based measurement can be performed. Image orientation involves determination of the position and attitude of each perspective center. As seen in Figure 8, this information is necessary for 3D computation by intersection of image rays. The determined orientation parameters allows for georeferencing of image features on the ground. In addition, individually acquired large number of images can be organized in correct order (sequence) to form image block in process of large areas and extraction of road features over road networks or road segments. Thus, automated image orientation is always a necessary a step in large area mapping of remote sensing and photogrammetry projects. While our low-altitude UAV systems is flexible to acquire imagery with higher overlap and fine ground resolution, it is more susceptible to air resistance, windy weather, mechanical vibrations etc. Therefore, the UAV cannot follow exactly the predefined flight mission for image acquisition, resulting in large variations of overlaps and orientations between adjacent images.

We have developed a robust approach to orient UAV-acquired imagery. The idea is to first determine the spatial relationship between a pair of stereo images using detected features commonly in the overlapped area. The stereo images serve as base. Then, expanding on the both directions, more images are linked iteratively and finally forming image block of the project area. The main challenges in the process for orientation of images acquired along a road or road network thus include automated relative orientation, formation of image block and bundle block adjustment of images. We start from relative orientation of stereo images to determine the relative angular and positional displacement between images that existed when the image was taken. For this purpose, we extract feature points using the SIFT algorithm (Lowe, 2004), and determine point correspondence by the comparison of the point attributes. With the conjugate points across images, the relative orientation of the stereo images is performed through the coplanarity principle. Afterwards, we compute the 3D model coordinates which are then employed to calculate the exterior orientation elements of the image immediately neighboring the stereo pair via space resection (Mikhail et al., 2001). The exterior orientation elements are further refined by a bundle adjustment procedure which also simultaneously updates the 3D model coordinates. To account for variations caused by irregular flight pattern of the UAV and errors of the correspondences, we applied L_1 -norm estimator in the computation of parameters. L_1 -norm estimator proves to be robust in identifying errors. The above process repeats iteratively and more images are added, while the block grows progressively until all images collected in the mission are integrated. A final bundle adjustment is conducted on the formed image block with the computed exterior orientation elements of each image as approximation. This results in accurate exterior orientation parameters which allows for stereo or multi-image mapping. Figure 10 outlines our developed procedures for image orientation. The whole procedures are detailed in the following sections.

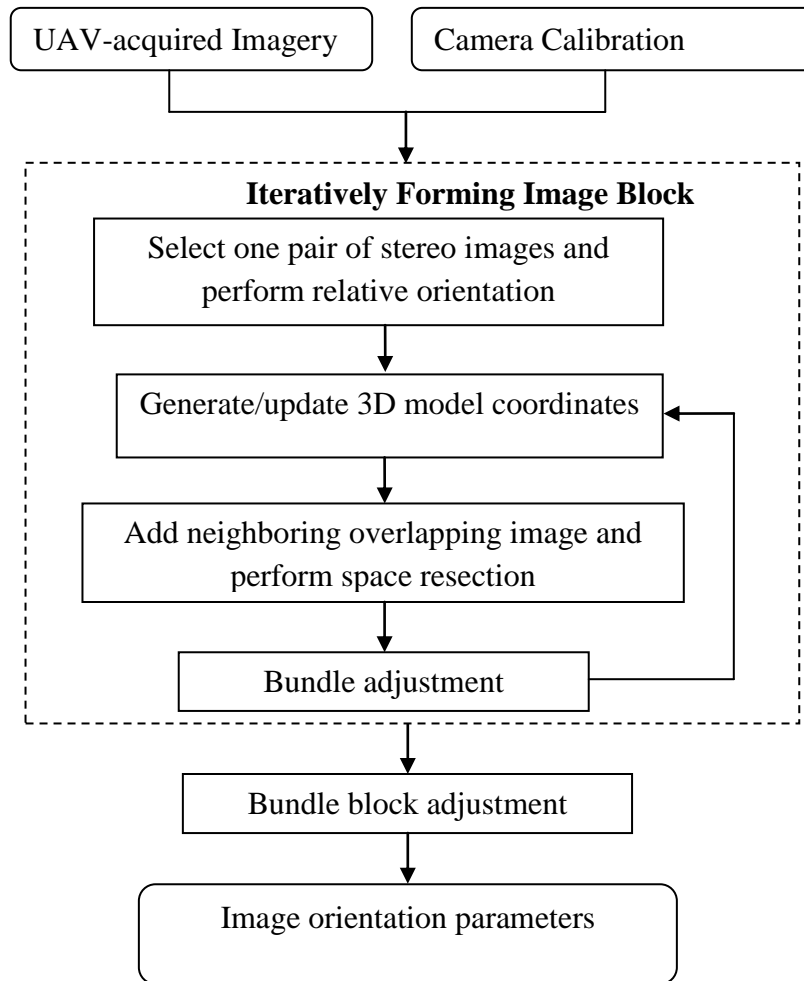


Figure 10. Outline of image orientation approach.

5.3 Feature Point Extraction and Matching

Automatic extraction of feature points and determination of correspondences across images are very important in image orientation. First, SIFT algorithm (Lowe, 2004) is employed to extract distinctive image points. These points are invariant to image scaling, translation, and rotation. The SIFT operator generates a 16x16 sample array around each keypoint, and the gradient magnitude and orientation are computed for each sample point. The gradient orientations are then accumulated into 128 orientation histograms summarizing the contents of 4x4 subregions. Finally, for each keypoint point, the SIFT operator computes 128 descriptor values in the range between 0 and 255. Figure 5 gives an example of extracted point features superimposed on the road image. The method works well, extracts distinct points both on road surface and road side features as demonstrated in Figure 11.

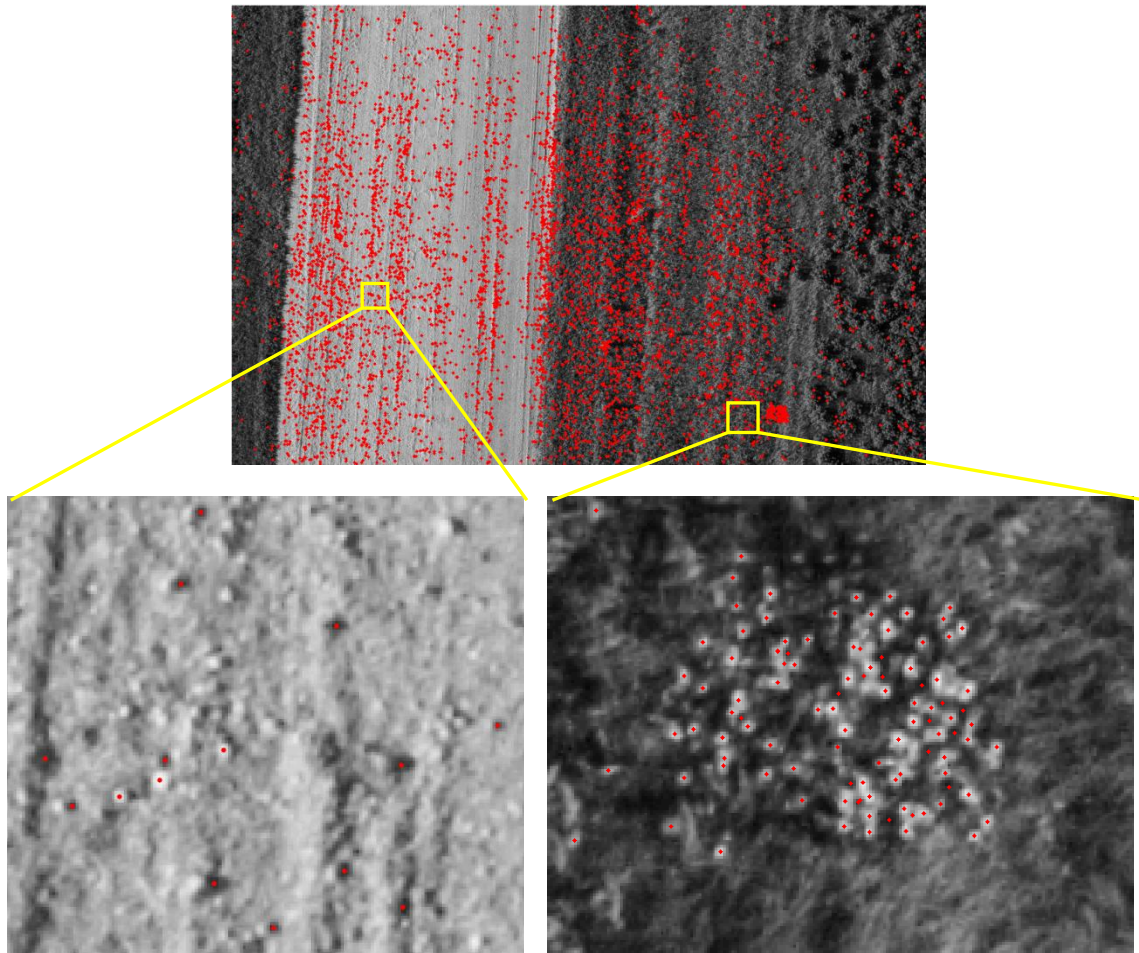


Figure 11. Extracted feature points (in red) by the SIFT method from a road image. The top image shows the overview of the performance. The details of the extracted points are presented in the bottom row in the original resolution of the image.

The extracted point features of each pair of images are matched based on the Euclidean distance of their descriptor vectors. A descriptor $D1$ in image (1) is matched to a descriptor $D2$ in image (2), if the Euclidean distance between the two descriptors multiplied by a pre-selected threshold is not greater than the distance of $D1$ to all other descriptors. This simple algorithm proved to be efficient in our project. Figure 12 shows the results of matching different image pairs in the along- and across-track directions of which only very few mismatches remain. In the figure, the extracted point features are presented in blue and red dots in stereo images, respectively. The mismatches are usually from the improper determination of the threshold. In addition, as the nature of the comparison of point attributes, any two different points with similar attribute will be most likely selected as conjugate points, since no other constraints such as image epipolar geometry are applied.

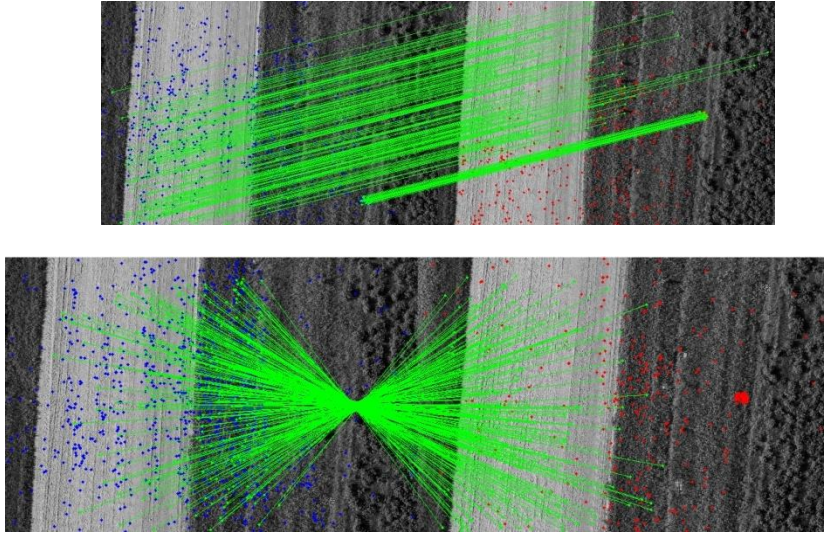


Figure 12. Results of matching two different image pairs in the along-track direction (top) and in the across-track direction (bottom). The green lines link the conjugate points in the image pair.

5.4 Relative Orientation

With the matched conjugate points between images, we determine relative orientation of an image pair, as the initial step to form the image block. The coplanarity condition is applied and a least-squares estimation model is performed to compute the relative orientation parameters of the two images. Inputs to the model are the image coordinates of the corresponding points in the two images, while outputs are the exterior orientation parameters of one image with respect to the second image. Since mismatches are unavoidable, a robust estimation able to account for correspondence errors is required. For this purpose, RANSAC procedure could be useful (Läbe and Förstner, 2006). However, RANSAC procedure has no upper bound on the time it takes to compute the parameters. Another disadvantage of RANSAC procedure is the need of setting problem-specific threshold. For these reasons we used the L_1 -norm estimator in our research. L_1 -norm minimization is capable of identifying gross errors in many systems of overdetermined equations when adequate redundancy exists. In our implementation, we start with a low threshold for image matching in order to include all the potential correspondences, and apply L_1 -norm to minimize the coplanarity-objective function and remove gross errors. With the remaining correspondences, we then repeat the L_1 -norm minimization procedure to further detect errors and refine the relative orientation parameters. This process is repeated until no more errors are detected. This procedure proved efficient in our current experience. Almost all the errors are detected and removed by the L_1 -norm estimator, except one type of mismatch of a pair of points which has very similar point attributes, and is also on the epipolar line of stereo images. This type of error does not affect the quality of relative orientation. But it will produce incorrect 3D model coordinates. However, it can be detected and removed in the space resection process described below.

We have applied the above procedure to relative orientation with dependent and independent methods (Mikhail et al., 2001) on stereo imagery acquired in along-track and across-track directions by our UAV system. The results are quite stable using either method. The posterior estimator of the reference variance (σ^0) for the relative orientation process was less than one pixel in image space after removing the outliers using the L_1 -norm estimator.

Following the computation of the relative orientation parameters of an image pair, the 3D model coordinates of conjugate points are computed via space intersection. The determined relative orientation of the stereo image and the 3D coordinates serve the base to form the image block. We then search for the image immediately neighboring the stereo image by examining common points in the overlap areas. Then, the exterior orientation elements of the neighboring image are calculated via space resection (Mikhail et al., 2001). Again, L_1 -norm estimator is applied to minimize the effect of incorrect 3D points resulting from the mismatches remained in relative orientation. A bundle adjustment is performed taking the calculated exterior orientation elements as approximation. This will further refine the exterior orientation elements and update the 3D coordinates. We then continue the *search-resection-bundle adjustment* process to iteratively integrate images to the block until no more images are left or the remaining images cannot be integrated due to null overlap because of poor flight mission by the light-weighted system. The details of the bundle adjustment are given in the following section.

5.5 Bundle Adjustment of Free Network

The collinearity equation (Equation 1) describes the relationship between the 3D coordinates of object space points, their image coordinates, and camera orientation parameters.

$$\begin{aligned} F_{1i}^j &= x_i^j - x_o + f \frac{U_i^j}{W_i^j} \\ F_{2i}^j &= y_i^j - y_o + f \frac{V_i^j}{W_i^j} \end{aligned} \quad (1)$$

Where: x_o, y_o and f are the camera interior parameters,

x_i^j and y_i^j are the corrected coordinates of point j in image i ,

$$\begin{bmatrix} U_i^j \\ V_i^j \\ W_i^j \end{bmatrix} = \mathbf{M}_i \begin{bmatrix} X^j - X_{ci} \\ Y^j - Y_{ci} \\ Z^j - Z_{ci} \end{bmatrix}$$

\mathbf{M}_i is the rotation matrix for image i ,

X_{ci} , Y_{ci} , and Z_{ci} are the exposure station 3D coordinates for image i ,

X_j , Y_j , and Z_j are the object space coordinates of point j .

The corrected image coordinates x_i^j , and y_i^j are computed as follows:

$$\begin{aligned} x_i^j &= \bar{x}_i^j - dr(\bar{x}_i^j) - k_2(r_i^{j^2} + 2\bar{x}_i^{j^2}) + 2k_3\bar{x}_i^j\bar{y}_i^j \\ y_i^j &= \bar{y}_i^j - dr(\bar{y}_i^j) - k_3(r_i^{j^2} + 2\bar{y}_i^{j^2}) + 2k_2\bar{x}_i^j\bar{y}_i^j \end{aligned}$$

where:

$$r_i^j = \sqrt{\bar{x}_i^{j^2} + \bar{y}_i^{j^2}} \quad dr = k_1 r^3$$

k_1 , k_2 , and k_3 are the radial lens distortion coefficients.

Seven constraint equations, among the 3D coordinates of object space points, are imposed to overcome the datum deficiency problem resulting from the lack of ground control points (Kraus, 1997). This is given in Equation 2.

$$\begin{bmatrix} 1 & 0 & 0 & 1 & 0 & 0 & \dots \\ 0 & 1 & 0 & 0 & 1 & 0 & \dots \\ 0 & 0 & 1 & 0 & 0 & 1 & \dots \\ 0 & Z_1 & -Y_1 & 0 & Z_2 & -Y_2 & \dots \\ -Z_1 & 0 & X_1 & -Z_2 & 0 & -X_2 & \dots \\ Y_1 & -X_1 & 0 & Y_2 & -X_2 & 0 & \dots \\ X_1 & Y_1 & Z_1 & X_2 & Y_2 & Z_2 & \dots \end{bmatrix} \begin{bmatrix} dX_1 \\ dY_1 \\ dZ_1 \\ dX_2 \\ dY_2 \\ dZ_2 \\ \vdots \end{bmatrix} = \begin{bmatrix} 0 \\ 0 \\ 0 \\ 0 \\ 0 \\ 0 \\ \vdots \end{bmatrix} \quad (2)$$

where:

X_i , Y_i and Z_i are the 3D object space coordinates of point i ,

dX_i , dY_i and dZ_i are the correction of the 3D ground coordinates of point i .

The final least-squares estimation model is solved in a unified approach (Mikhail and Ackermann, 1976), where all unknowns involved in the adjustment procedure are considered observations. However, differentiation between real, i.e. image coordinates, and pseudo observations, i.e. orientation parameters and ground coordinates, is presented in the covariance matrix of each group. Observations assigned with low variances are considered fixed during the adjustment and are not allowed to change freely. On the other hand, observations assigned with high variances are allowed to be adjusted freely. Equation 3 represents the final least squares estimation model.

$$v_{n \times 1} + B_{n \times (3m+6p)} \Delta_{(3m+6p) \times 1} = f_{n \times 1} \quad (3)$$

$$\begin{bmatrix} C \\ 0 \end{bmatrix}_{7 \times 3m} \Delta_{(3m+6p) \times 1} = 0_{7 \times 1}$$

where:

n is the number of rays in the image block multiplied by 2,

m is the number of ground points,

p is the number of images

v is vector of residuals for the image coordinates,

B is the coefficient matrix,

C is the coefficient matrix of the constraint equations,

f is the vector of numerical values ,

Δ is the vector of unknowns.

The final solution for the model is presented by Equation 4.

$$\Delta_{(3m+6p) \times 1} = (B^t W_e B + C^t W_{ec} C + W_{xx})^{-1} (B^t W_e f - W_{xx} f_x) \quad (4)$$

where:

W_e is the weight matrix for the image coordinates,

W_{ec} is the weight matrix for the constraints,

W_{xx} is the weight matrix for the unknowns,

f_x is the difference between the approximate values and the adjusted values at each iteration,

other symbols are defined in Equation 3.

5.6 3D Reconstruction and Measurement of Surface Distresses

One of the key elements of image analysis in the system is 3D reconstruction of the road surface from which the surface distresses can be detected and the dimension and size can be measured. We have developed an efficient approach to process the UAV-acquired imagery to derive 3D

road surface fully automatically using the combination of digital photogrammetry and computer vision techniques. Since a point on a road is captured in consecutive images, thus, by reversing the imaging process, its 3D position can be computed through the intersection of the image rays (Figure 13). The fundamental process to automate this procedure is to locate the corresponding points in image space. This is achieved by automated image matching.

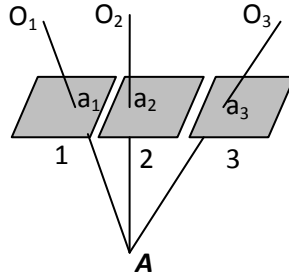


Figure 13. Imaging process and 3D reconstruction from images. Ground point A is imaged at a_1 , a_2 and a_3 in images 1, 2 and 3 respectively from perspectives O_1 , O_2 , O_3 . Point A can be reconstructed by the intersection of image rays of O_1a_1 , O_2a_2 , and O_3a_3 .

Due to the inherent errors in the image orientation and the camera calibration, the 3D positioning accuracy is associated with the intersection angle. The uncertainty is higher with small intersection angles. Thus, for 3D reconstruction purpose, we seek for images with larger separation. However, with increasing separation, image distortion is large. This creates difficulty in automated matching for point correspondences. To solve this problem and efficiently use the UAV-acquired images, we first conduct image matching in immediately neighboring stereo images (e.g. 1 and 2, 2 and 3 in Figure 13) to find the correspondences (e.g. a_1 and a_2 , a_2 and a_3). Since the image distortion is small between images 1 and 2, the matching success rate is high. Thus, by fusing the matching results, we also determine the correspondences between images with larger separation (e.g. a_1 in 1 and a_3 in 3). For the computation of the 3D point A on the ground, we employ a weighted multiple image ray intersection approach (Mikhail et al., 2001) which involves all the images containing point A . The weight is determined with the proportion to the image separation. Therefore, in the case shown in Figure 13, three image rays are intersected, while the highest weight is given to the image rays O_1a_1 and O_3a_3 . This strategy efficiently explores consecutive images for image matching and 3D computation, thus providing reliable and accurate 3D model of road surface, necessarily for measurement of surface distresses.

Although we have used images with less distortion for image matching, however, automated image matching is still an active research topic in photogrammetry and computer vision for automated mapping (Zhang, 2003), city modeling (Lafarge et al., 2008), object construction and recognition (Chehata et al., 2009), engineering applications (Wang et al., 2007; Chi et al., 2009), etc. In this work, we use a coarse-to-fine hierarchical strategy with several image matching

algorithms (Zhang and Fraser, 2008). The road surface model is constructed by combining the matching results of feature points, grid points. The coarse-to-fine strategy has been designed to initially reconstruct the surface model from matched feature points. Afterwards, evenly distributed grid points are used, with the matched grid points improving the initial surface model in areas with poor or no texture. The outcome is a road surface model with dense 3D points and this forms the detailed shape of the road surface.

The 3D points generated in the process of image orientation, although sparsely distributed along the road segment, deliver a rough road surface model. This model serves as initial value in grid point matching using cross-correlation technique. A regular grid is produced for the road segment. Therefore, each grid point has a fixed X and Y coordinates, and its initial Z coordinate can be derived from the generated rough surface model. To precisely determine the Z value, image matching with cross correlation technique has been developed and outlined in Figure 14. Assume A is a grid point with fixed horizontal coordinates X_A , Y_A and initial Z value Z_0 . The vertical coordinate of A is Z_A and is in the range $(Z_0 - \text{delt}Z, Z_0 + \text{delt}Z)$. A is photographed at a_1 and a_2 in images 1 and 2, respectively. Since Z_0 differs from Z_A , the projections of (X_A, Y_A, Z_0) to images 1 and 2 (the black dots) deviate from a_1 and a_2 in the images. Thus, the image patches around the projections demonstrate large difference and therefore cross correlation on the image patches deliver a small coefficient which describes the similarity of the image signals. Cross correlation will achieve the largest value when Z_0 is replaced with Z_A . Based on this principle, we alternate the Z value from $Z_0 - \text{delt}Z$ through $Z_0 + \text{delt}Z$ progressively. At each step, we perform cross correlation on the image patches around the projection points and record the correlation coefficients. We then determine the correct vertical coordinate of point A and correspondence across images based on the largest correlation coefficient.

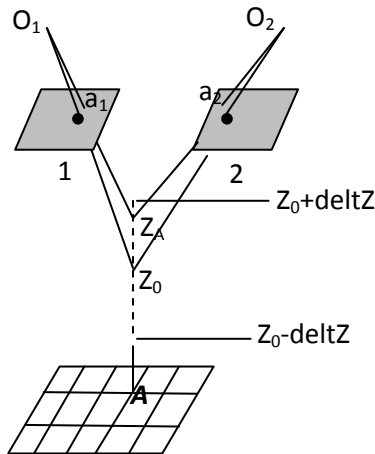


Figure 14. Determination of Z coordinate of grid point A (X_A , Y_A) with initial Z value Z_0 . Z_A is in the range $(Z_0 - \text{delt}Z, Z_0 + \text{delt}Z)$.

The above procedure delivers correspondences with pixel level accuracy. We finally conduct a multiple image least squares matching (Elaksher, 2008) to further refine the matching results providing sub-pixel accuracy of point correspondences, thus further improving the quality of the Z coordinate of the grid points.

In least squares matching, for a window of N points the intensity difference in each pair of images for each point should, ideally be, equal to zero. The previous statement can be stated as the condition equation in the least squares adjustment process. Equation (5) shows the mathematical form of this condition equation.

$$G_{ij}^{pq} = g_{ij}^p - g_{ij}^q = 0 \quad (5)$$

where

G_{ij}^{pq} is the least squares matching equation,

g_{ij}^p , g_{ij}^q are gray values for one pixel representing post (i,j) in images p and q respectively.

The gray level in each image is the function of the position of the pixel. Hence, the adjusted pixel location could be determined. This is achieved by minimizing a goal function, which measures the differences between the gray levels in the template and the patch images. The goal function to be minimized is the L_2 -norm of the residuals of the least squares estimation.

The above process is repeated for each grid point and thus produces high quality road surface model with dense grid points. The density of the model can be adjusted by changing the interval of the grid, thus this approach is also suitable for various engineering applications requiring different resolutions of 3D surface data.

Chapter 6 Experiment Tests

The developed system has been tested over several rural roads near Brookings, South Dakota. During data acquisition period, the roads demonstrated moderate distresses such as potholes or ruts. In following, after a brief review of the test site, we present image acquisition procedure. The acquired images were then analyzed to determine orientation parameters. Afterwards, the developed 3D reconstruction approaches were applied to generate 3D models of potholes and ruts. Meanwhile, the ortho-rectified images were produced. We finally present the measurements of potholes and ruts from the generated 3D models and orthoimages.

6.1 Test Site Description

Though we have flown our UAV in some rural areas near the town Brookings, SD and acquires images over a number of unpaved road segments, we have finally decided our test site five miles west of the town. This decision was made after frequent contact and consult with the Brookings Council, Police Office, Sheriff and Brookings Highway Department. We have participated in the regular Brookings local road maintenance meetings and received supports from the maintenance teams in the region. We then travelled around the rural road network and investigated and inspected roads and decided the test site. A snapshot of the test site is presented in Figure 15.

This small community locates in an agricultural area. It has a few farms and consists of eleven roads. These roads experience heavy traffic during late spring, summer and early fall, and connect farms to local towns and outside markets. While small, the site represents a typical farming community in agricultural regions. The roads are usually completely covered by snow and ice during winter. The conditions are generally bad after snow thaws in spring. Extensive maintenances are usually required in planting and harvest seasons. However, evaluation of road condition is rarely performed. Thus, maintenance is conducted based on the very limited windshield surveys or complaints of the local residences. Based on discussions with farmers and local road maintenance teams, this site is typical and representative, and thus is well suited as a test and validation site in our project. Figure 16 presents several examples of road images in this community taken in middle of May 2009. The surface distresses are clearly presented in the images.



Figure 15. Test site.





Figure 16. Examples of road image in the selected test site.

6.2 Image Acquisition

Flight plan is performed on the weGCS on ground control station. A georeferenced raster map of the mission site is loaded in the software. The mission parameters can be set interactively on screen. The results of flight plan are flight route, definition and locations of waypoints, flying parameters such as flight height, speed in the course of the journey.

The UAV helicopter can be navigated both by weGCS and a human pilot. Usually take-off and landing were controlled by the pilot in so-call assisted mode, while the actual flight mission was navigated by weGCS in fully automatic mode following the planned flight mission. Based on the plan, the UAV traveled along the defined route passing through designed waypoints after assisted take-off. During the course, the camera was automatically triggered to capture road image with defined overlap from the first waypoint to the end of the mission. The system status was presented on GCS, allowing for system monitoring and intervention wherever necessary.

In tests, the UAV flew at an altitude of about 45m above ground, capturing details of the road surface with image scale of ~900. The ground resolution is about 5mm. The UVA travelled at 4m/s, acquiring road images with 60% overlap along the path. Figure 17 is an example of the road imagery collected over a road segment with ruts. This road segment was imaged four times in a single mission, providing highly redundant information for the evaluation of road condition, and also allowing for precise 3D measurement of road surface features. Thanks to the very high spatial resolution, the fine details of the road surface distresses are clearly presented in the image, allowing for detailed evaluation of the road surface condition.

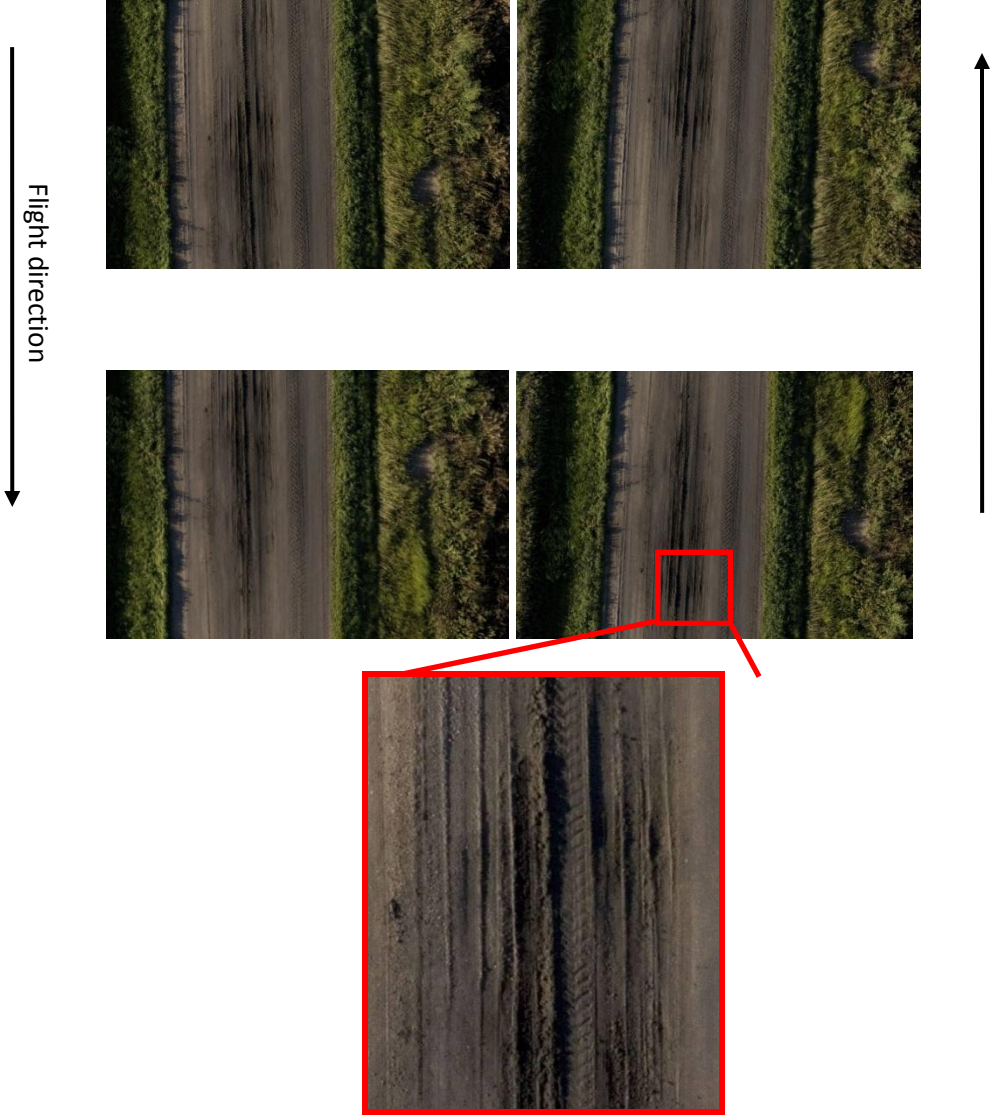


Figure 17. Example of road images acquired by UAV over a road segment. The segment was captured 4 times in a single mission. The flight directions are indicated by arrow lines. The bottom image shows the fine details of road feature (ruts) in original resolution.

Figure 18 is another imagery collected by UAV allowing for evaluation of culvert.

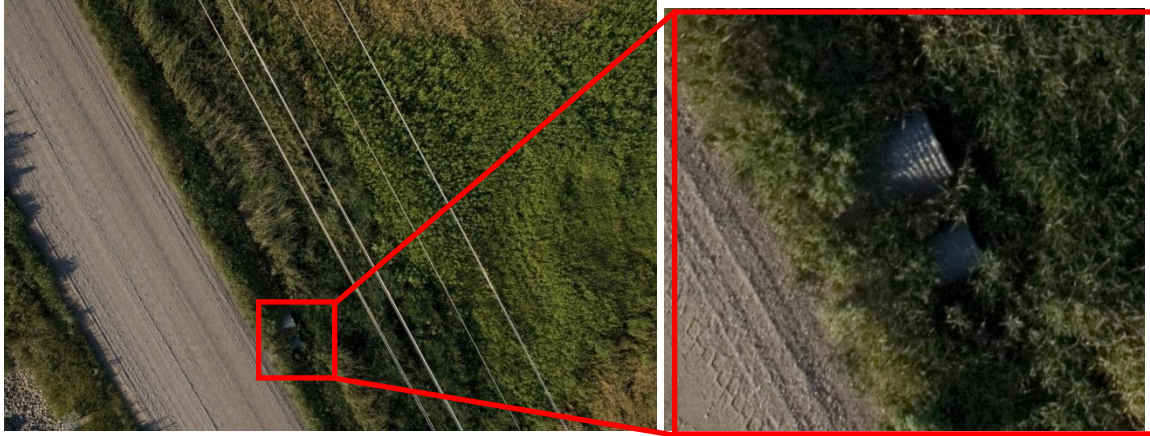


Figure 18. UAV acquired image allows for evaluation of culvert. Left: road image in reduced resolution. Right: culvert in original resolution.

Road shown in Figure 19 demonstrate severe ruts. Note we have designed some marks to facilitate ground survey and relate the ground measurements with image measurements.



Figure 19. Road image acquired by UAV showing severe ruts. Note the marks are designed for ground measurements and for relating ground measurements with image measurements.

The system also recorded flight data, such as GPS, INS observations. We observed that the helicopter UAV did not follow exactly the predefined path during the missions. The actual route varies as a result of disturbances such as air resistance, wind, vibration etc. Poor along-track overlap (~20%) has been observed. This has posed challenges for image orientation and 3D reconstruction.

6.3 Image Analysis for 3D Reconstruction for Measurement of Surface Distresses

Image Orientation

Following the procedures described in the Section 5.2, the relative orientation process is first performed using a pair of stereo images and the 3D object space coordinates of conjugate points are then computed via two image intersections. Afterwards, new images are added sequentially and a free network bundle adjustment is performed to update the exterior orientation parameters and the object space coordinates. Each time a new image is added, the algorithm locates its point features, find their correspondent points in all previous images, and adds the new set of points in the image block. The free network bundle adjustment then computes the exterior orientation parameters of the images and update the 3D coordinates of the object space points. Figure 20 shows the results of each stage for a 14-image block.

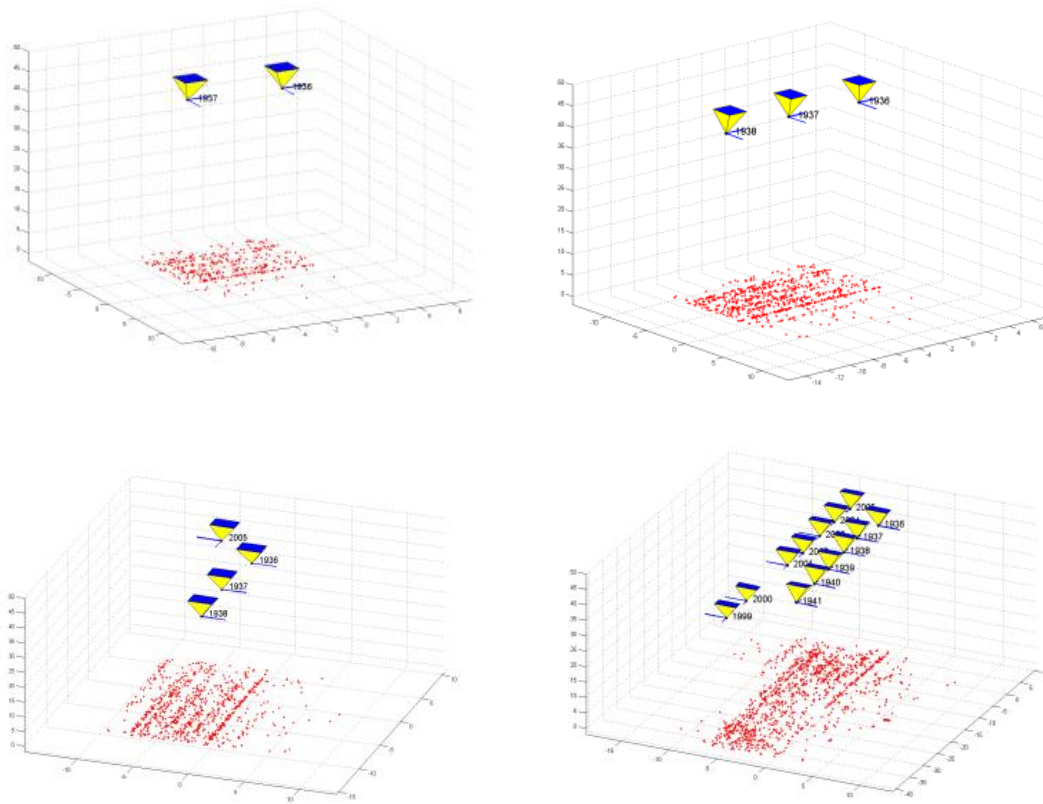


Figure 20. 3D view of automatic image block formation and image orientation. Top-left shows relative orientation of an image pair. Then, the block is progressively growing by integrating more images (top-right and bottom-left) until no more images are left and the final image block is formed (bottom-right). The object space points are shown in red.

The performance of the approach is robust as shown in Figure 21 where the residuals are presented. It is clear that for most of points the residuals are within 1 pixel. Large residuals remain only on a few points. This might be caused by incorrect or imprecise point match, and may be eradicated by robust outlier removal.

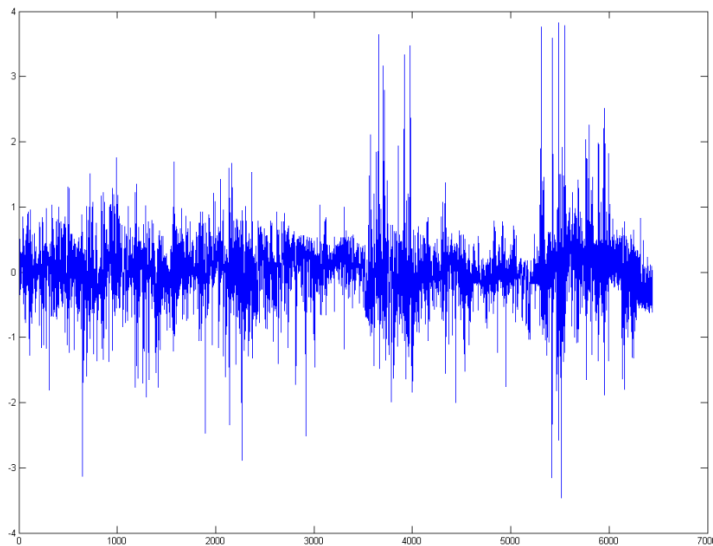


Figure 21. Residual of bundle adjustment on the image block in Figure 20.

3D Reconstruction of Ruts and Potholes

The developed 3D reconstruction algorithms were applied to the acquired imagery for 3D measurement of surface distresses, such as ruts and potholes. Figure 22 (left) shows an image patch of rut on a road section. Field survey with tape shows the distress is very mild with the depth of the hole around 2 inches. After manual identification of the rut in images, a regular grid was generated. Image matching was then performed using the techniques described in Section 5.6. With the determined image orientation parameters, the 3D positions of the road points were computed. This resulted in dense 3D points allowing for precise description of the shape and size of the rut as shown on the right of Figure 22.

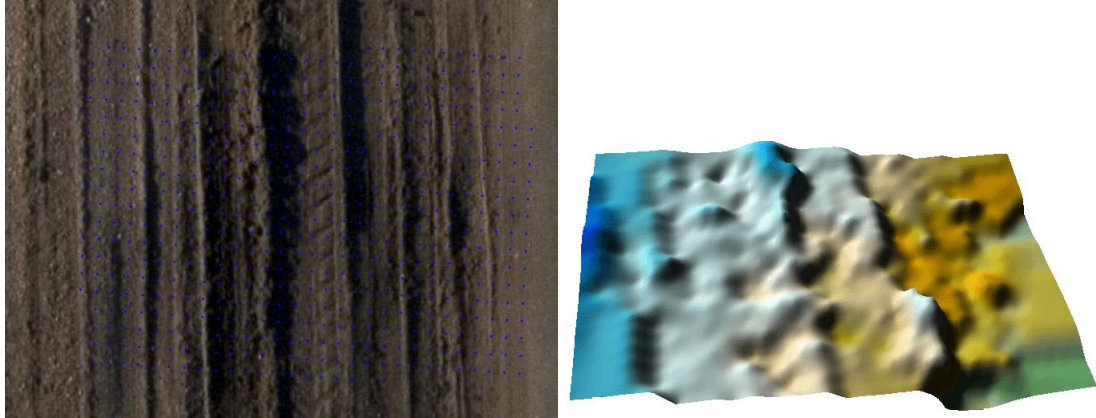


Figure 22. 3D reconstruction of rut. Left: an image patch of rut on a road. The blue dots represent grid points. Right: reconstructed 3D model of the rut area.

The similar procedures were applied to a road segment with mild potholes. An example is given in Figure 23. The top row of the Figure 23 shows the ground shot of the pothole and the field measurement of the depth using a tape. It is clear this is a mild distress with the depth less than 2 inches. However, the developed approach has successfully generated the 3D shape (bottom row, right) from the UAV acquired images (bottom row, left). Figure 24 is another example.



Figure 23. 3D reconstruction of pothole from UAV-acquired imagery. Top: ground shot of pothole (left) and field measurement (right). Bottom row: image of pothole photographed from UAV (left) and its 3D model (right) produced from imagery.

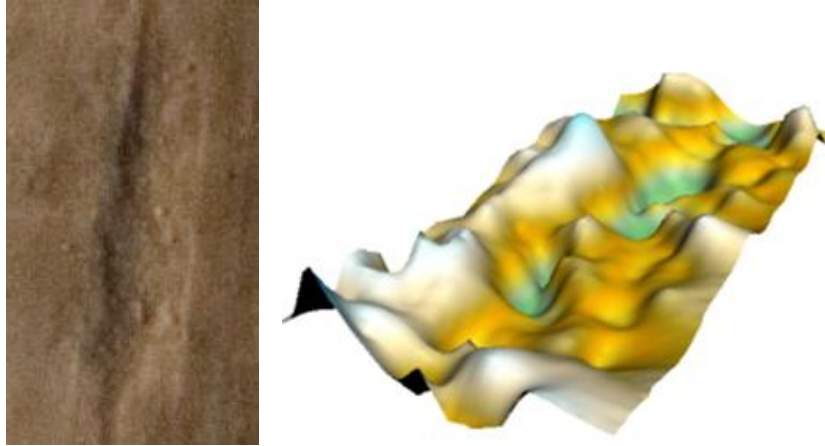


Figure 24. 3D reconstruction of pothole from UAV-acquired imagery. Left: image of pothole photographed from UAV. Right: its 3D model produced from imagery.

Generation of 3D Images

With the determined orientation parameters of images and the reconstructed 3D surface, the orthoimages and 3D road images can be generated. Orthoimages can be used for precise measurement in two-dimension space. Orthoimage and 3D images are particularly useful for visualization. For production of orthoimages, a regular grid is generated in ground space. The coordinates for each grid point can be derived from the reconstructed 3D surface. Each grid is then back projected to image space using the image orientation parameters. The color information at the projection point is taken to paint the grid and thus producing orthoimage. To generate 3D image of road surface, the 2D image is draped onto the reconstructed surface again using the orientation parameters. Since 3D image is a virtual representation of object, it is more attractive for visualization. The 3D images can be further treated to generate video product which provides virtual tour of the roads. This allows for more detailed visual inspection of roads on computer. Examples of the generated 3D road images with different perspectives are shown in Figure 25.



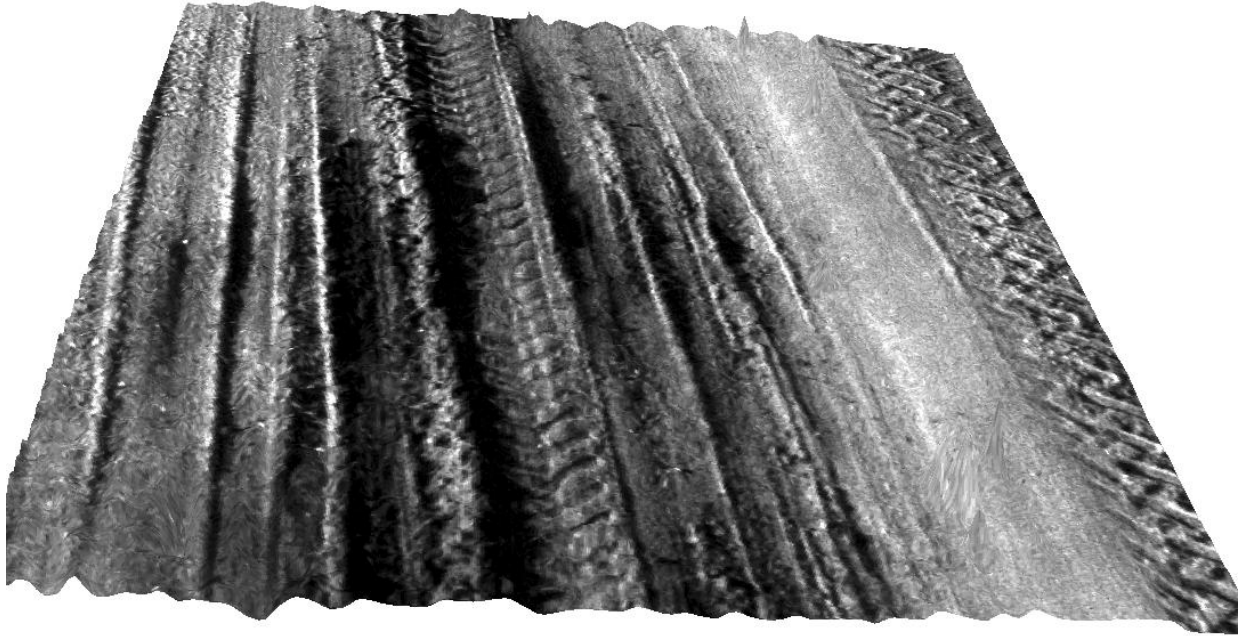




Figure 25. Reproduce of 3D image of road with severe distress from UAV-acquired imagery.

Distress Measurements

Based on the 3D models and orthoimages of ruts and potholes, the distress properties, such as depth and size can be measured. This is done in GIS software Arcmap. The maximum depths of the ruts and potholes in Figure 22 and Figure 23 are 6.5 cm and 3.5 cm respectively. Comparison with field survey with tape was also conducted. The differences between image-based measurement and field survey are within the range of 1 cm, demonstrating good performance of the system. In addition to depth, other important parameters in road condition assessment, such as the size and extension of potholes and ruts can also be easily measured with a few mouse clicks. Examples are shown in Figure 26.

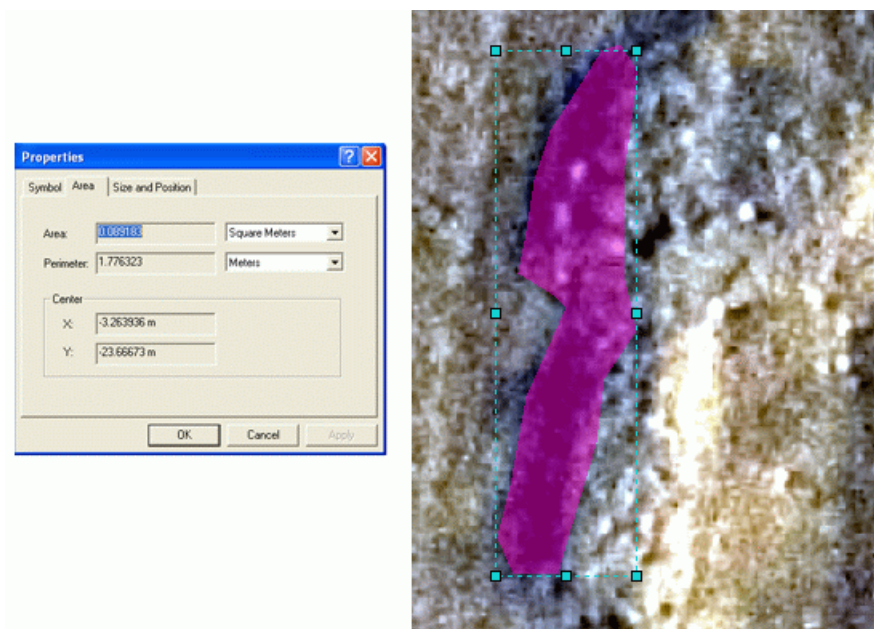
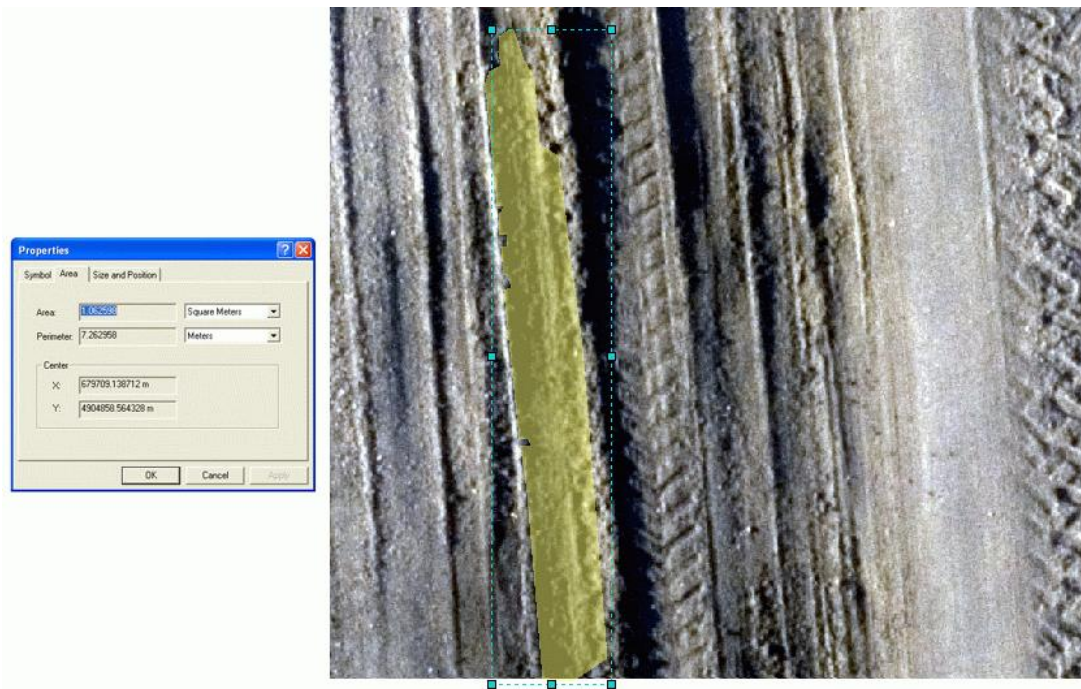


Figure 26. Measurement of the size of ruts (top) and potholes (bottom).

6.4 Accuracy Analysis

Theoretically, the planimetric precision σ_{xy} of photogrammetric measurements of single point is a function of image measurement precision σ_{img} and image scale S.

$$\sigma_{xy} = \sigma_{img} * S \quad (6)$$

The precision of height σ_z depends on image measurement precision σ_{img} , image scale S and the ratio between UAV flight height H and the spatial separation of the stereo images B. It is given as:

$$\sigma_z = \sigma_{img} * S * H / B \quad (7)$$

It can be seen the precision of height is affected by flying height. In addition, the overlap between the images also plays an important role. Lager separation delivers higher accuracy.

Equations (6) and (7) indicate the precision of single point measurement. The precision of distance between two points in planimetry and height is then determined through error propagation, and is given in Equation (8) and (9) respectively.

$$\sigma_L = \sqrt{2.0} * \sigma_{xy} \quad (8)$$

$$\sigma_{\Delta Z} = \sqrt{2.0} * \sigma_z \quad (9)$$

In our experiment, the road images are acquired with a 60% overlap at 45m above ground. The spatial resolution of image is ~5mm, and the average spatial separation between stereo images is around 6.5m. With camera focal length of 50mm, the image scale is ~900. Assuming image measurement accuracy of 0.2pixel, the theoretical precisions of point determination in planimetry and height will be around 1mm and 7mm respectively. Apparently, this theoretical precision gives an overall picture of the capability of the system. The performance of the system should be assessed by the actual accuracy determined by the comparison between image-based and ground measurements.

During our flight missions, ground measurements are were also taken. The measurement was done using tapes, rules. Thus, the measurements are not always very accurate. Nevertheless, the comparison on two short road segments indicated that the differences between the measured depths of ruts are within 1cm. Although limited data collected due to hardware failure, this result indeed shows the excellent system performance.

Chapter 7 Discussions

In this report, we have presented the developed UAV-based remote sensing system for road condition data acquisition. The system consists of a UAV helicopter integrated with GPS/IMU and a digital camera, and a set of image analysis algorithms.

This inexpensive light payload helicopter uses electric engine which reduces vibration compared to the counterparts of gas engine, thus allowing for stable quality of images. The inexpensive amateur camera Canon Rebel XTi can provide adequate quality for the documentation of the fine details of road surface. The nice component of this system is the flight control system. FCS plays an important role. It enables flight route programmed in office, fuses the observation of GPS/IMU during mission to navigate the helicopter to follow the plan, and triggers camera to capture images with specified parameters.

The disadvantage of this electric engine helicopter is that the endurance is usually short due to limited capacity of battery. The UAV is more susceptible to wind due to its light weight. The critical part is the design, careful selection of materials, proper arrangement of sensors and other components so that damaging events such as short circuit never happen. For instance, carbon frames should be avoided, wires should be wrapped properly and antenna of sensors on board should be well arranged to avoid signal interference. This is one of the most important lessons we learnt from this experience as our helicopter crashed in one mission due to short circuit. However, given limited funding, this flexible system is still considered to be well suited for research with some improvements.

The developed image analysis algorithms prove to be robust to process UAV acquired imagery. The major algorithmic development includes integrated sensor orientation, 3D reconstruction and semi-automatic measurement. The sensor orientation approach determines the image orientation parameters fully automatically. Starting from relative orientation of stereo images, the image block of the entire road segment is formed by repeatedly augmenting new images. To achieve highest accuracy, we applied robust L_1 -norm estimator to account for errors and bundle adjustment and bundle block adjustment techniques to ensure consistency. As shown in the test, the residuals with several datasets are within 1pixel, indicating the robust performance of the algorithms.

3D reconstruction of road surface is the key to the success of distress measurement. Indeed, 3D data of road can also be used to derive other road properties such as slope, geometry (width, radii), and locate road side features. We have developed an improved 3D reconstruction approach. Algorithm wise, image correlation has been applied to generate an initial model which is further refined by least squares image matching to achieve sub-pixel accuracy. Strategically, we follow a coarse-to-fine approach. Image matching starts from the top of image pyramid to produce a rough model but with less or no errors. Then, image matching and 3D reconstruction propagate from the top of the pyramid to the bottom to iteratively improve the surface with more

and more details. To fully benefit from multiple images available from our UAV system, we relay image matching results among overlapped images, and treat images differently in image ray intersection by assigning different weights to each individual ray. The results presented in Chapter 6 shows the good performance of the approach. The road surface features are nicely reproduced. The method can be improved in some aspects. Currently, the threshold in image correlation is set manually. Robust adaptive threshold may results in less errors and thus better quality of surface model. The procedure of least squares image matching is slow due to large matrix computation and iterative process. This may pose challenge when a large number of images in a big road network are to be processed. Powerful computer such as supercomputer should help.

The quality of 3D reconstruction can be further improved if the UAV helicopter is upgraded and more advanced cameras are used in future. A gust of wind can push our helicopter away from the planned road. This may cause smaller image overlap thus decrease the geometric strength of the image block. This can be avoided if a stronger machine is used. With the advancement of camera technology, new high quality camera may be adapted. With higher spatial resolution, the flight height can be increased without loss of fine resolution of images, and larger area can be covered in each image. This will reduce the cost of the data management, and increase the 3D reconstruction accuracy since the spatial separation of images is getting larger.

Currently, the measurement of distress is performed semi-automatically. While it is a useful approach, this labor work should be replaced in future with automatic methods.

The major limitation of current system is that some distresses cannot be observed, such as inadequate roadside ditches, dust. Ditches are usually covered by grass and cannot be sensed by camera. This may be solved by a lidar sensor penetrating through grass. Such sensor can be easily integrated in the current system if sufficient funding is available.

Chapter 8 Conclusions and Recommendations

Conclusions

Rural road network is the lifeline of agricultural activities and link agricultural communities to nearby towns and markets. Thus, road condition data is important in local transportation management, and road condition is also critical to safety and farming activities. At present, essential information about the existence, locations, dimensions, and condition of roads is typically collected in slow, dangerous, and expensive manual processes. This significant cost-in both time and money- has caused many local agencies to rely on visual inspection, intuition and occasional spot measurement in their assessment. Yet, the importance of timely identification and rectification of road deformation cannot be overstated.

This research developed a UAV-based remote sensing system for road condition data acquisition. This low-cost flexible system is easy to operate, and can efficiently capture road imagery fully automatically. Developed image processing algorithms then analyze the acquired images for image orientation, generation of 3D models of road surface and ortho-rectified road images which allows for extraction of road surface distresses (potholes, ruts etc) with more details. Quantitative measurements are conducted in office with computer-aided techniques. Thus, in contrast to conventional road condition data collection approaches, this system does not require field work. Even field visit is not needed. Therefore, it enables local agencies more quickly, efficiently and safely collect data needed for rural road condition assessment. Since the road data are documented in digital imagery, re-measurement is possible whenever is necessary. The generated 3D road images enable better visualization and inspection of road features. They can be easily integrated as video products for virtual roads. In addition, the acquired digital imagery of roads, together with the extracted road condition data, and the derived products can be directly integrated into road management system.

The proposed system has been tested over a number of rural roads with various surface conditions. Road images has been acquired with ground resolution as high as 5 mm, allowing for identification and detailed evaluation of road surface condition including distress type, severity and extent. The developed 3D surface reconstruction approach has been applied to the acquired imagery, and the 3D shapes of surface distresses such as potholes, ruts have been generated. A semi-automatic approach then allows for accurate measurement of extent of the distresses three-dimensionally on computer. Meanwhile, manual field measurements were conducted during flight mission to establish ground truth for testing the accuracy of the proposed system. The results show that the image processing algorithms works well on the UAV-acquired road imagery to measure the road surface distresses.

In conclusion, this research has demonstrated the capability of UAV-based remote sensing for rural road condition data collection. The developed system can provide detailed and accurate

measurements of road surface distresses, and thus improving the efficiency of road condition data collection.

Recommendations

To make the developed system serve transportation agencies, further research may be directed to:

- Extensively test the developed system over a diversity of regions to validate the performance in terms of accuracy and efficiency. Due to limited data collection in this phase, the time and cost associated with image-based condition data collection were not adequately documented. From the limited experience, the field work required for UAV flight is significantly low compared to ground survey. However, the save of time and cost is not fully clear yet.
- Further development of automated methods for distress measurement. Currently, the image orientation and surface model production are carried out by computer with high quality. However, the measurements for length, depth and area are performed semi-automatically on computer. Further research will focus on new robust approaches to automatically identify various distresses on roads.
- With the advancement of UAV and sensor technologies, more powerful and safer inexpensive UAVs will emerge onto market. Such UAVs will supply longer endurance in mission to serve larger community. Inovatve sensors, such as infrared cameras, Lidar can be integrated to the current system. This will allow for more efficient road condition assessment in fully automatic mode.

In addition to collect surface distress data, the developed UAV-based remote sensing system can be also used to collect other transportation asset. One of the further researches submitted to USDOT by us recently has been documented in a white paper in response to US DOT DTOS59-08-RA-00002. That white paper has been accepted by USDOT in which we propose to further develop our system to collect road images and quantify other road condition parameters including length, width, slope, radii, curvatures of unpaved roads, geolocation of roadside features (trees, utility poles, buildings), drainage features (culverts, bridges), and other small structures, and their distance to the edge of roadway. Such information, together with surface condition data, constitute the critical component of rural road management system which allows state DOTs and local authorities to manage their road networks more efficiently.

REFERENCES

Ameri, B., Meger, D., Power, K. & Gao, Y. (2008), UAS applications: disaster & emergency management, in *Proceedings of America Society of Photogrammetry and Remote Sensing Annual Conference*, Baltimore, MD, CDROM.

Baltsavias, E.P., Sullivan, L. & Zhang, C. (2004), Performance comparison between aerial imagery, ADS40 and IKONOS data for automated road centreline extraction using the ATOMI road network updating system. *International Archives of Photogrammetry and Remote Sensing*, 12-23 July, Istanbul, CDROM.

Baltsavias, E.P. & Zhang, C. (2005), Automated updating of road databases from aerial images. *International Journal of Applied Earth Observation and Geoinformation*, 6(3-4):199-213.

Chehata, N., Jung, F. & Stamon, G. (2009), A graph cut optimization guided by 3D-features for surface height recovery, *ISPRS Journal of Photogrammetry and Remote Sensing*, 64(2), 193-203.

Chi, S., Caldas, C.H., & Kim, D.Y (2009), A methodology for object identification and tracking in construction based on spatial modeling and image matching techniques, *Computer-Aided Civil and Infrastructure Engineering*, 24 (2009), 199-211.

Coifman, B., McCord, M., Mishalani, M. & Redmill, K. (2004), Surface transportation surveillance from unmanned aerial vehicles, in *Proceedings of the 83rd Annual Meeting of the Transportation Research Board*, Washington D.C.

Cronk, S., Fraser, C., & Hanley, H. (2006), Automatic metric calibration of colour digital cameras, *The Photogrammetric Record*, 21(116):355-372.

Eaton, R.A. & Beaucham, R.E. (1992), Unsurfaced road maintenance management, US Army Corps of Engineers Special Report 92-26.

Eisenbeiss, H., Lambers, K., Sauerbier, M. & Zhang, L. (2005), Photogrammetric documentation of an archaeological site (Palpa, Peru) using an autonomous model helicopter, in *Proceedings of the XXth CIPA International Symposium*, Torino, Italy, CDROM.

Eisenbeiss, H. (2006), Applications of photogrammetric processing using an autonomous model helicopter. *International Archives of Photogrammetry, Remote Sensing and Spatial Information Sciences*, Paris, France. CDROM.

Elaksher, A. (2008), A multi-photo least squares matching algorithm for urban area DEM refinement using breaklines, *International Archives of Photogrammetry, Remote Sensing and Spatial Information Sciences*, Beijing, China, CDROM.

Fraser, C.S. (1997), Digital camera self-calibration. *ISPRS Journal of Photogrammetry and Remote Sensing*, 52(4): 149-159.

Fraser, C.S., Dial, G., J. & Grodecki, J. (2006), Sensor orientation via RPCs. *ISPRS Journal of Photogrammetry and Remote Sensing*, 60(3): 182-194.

Gruen, A., Beyer, H. A. (2001), System calibration through self-calibration, in *Calibration and Orientation of Cameras in Computer Vision*, Springer, Heidelberg, 34: 163-193.

Gunaratne, A., Mraz, A., Sokolic, I. & Nazef, A. (2003), Development of Florida's comprehensive pavement evaluation vehicle, in *Proceedings of 82rd Annual Meeting of the Transportation Research Board*, Washington D.C., CDROM.

Hartley, R., & Zisserman, A. (2000), *Multi-view Geometry in Computer Vision*, Cambridge University Press, Cambridge.

Herold, M., Roberts, D.A., Smadi, O. & Noronha, V. (2004), Road condition mapping using hyperspectral remote sensing, in *Proceedings of the 2004 AVIRIS workshop*. Pasadena, CA, CDROM.

Herwitz, S.R., Johnson, L.F., Higgins, R.G., & Dunagan, S.E. (2002), Precision agriculture as a commercial application for solar-powered unmanned aerial vehicles. AIAA, Portsmouth, VA.

Kenneth, H.M. (2004), NCHRP synthesis of Highway practice 334: automated pavement distress collection techniques. Transportation Research Board, National Research Council, Washington, D.C., 94p.

Kontitsis, M., Tsourveloudis, N., & Valavanis, K.P. (2004), A UAV Vision System for Airborne Surveillance, in *Proceedings IEEE International Conference on Robotics and Automation*, Vol. 1, 77-83.

Läbe, T. & Förstner, M. (2006), Automatic relative orientation of images. In *Proceedings of the 5th Turkish-German Joint Geodetic Days*, Berlin, Germany, CDROM.

Mikhail, E.M. & Ackerman, F. (1976), *Observations and Least Squares*. IEP-A Dun-Donnelly Publisher, New York.

Mikhail, E.M., Bethel, J.S. & McGlone, J.C. (2001), *Introduction to Modern Photogrammetry*, John Wiley & Sons, Inc. New York.

NCRST (2000), Report of a Conference on Remote Sensing for Transportation. Washington D.C.

NCRST (2003a), Accomplishments 2003. available at: <http://www.ncgia.ucsb.edu/ncrst/synthesis/SynthRep2003/>. Accessed on 12 June, 2006.

NCRST (2003b), MidWest Regional Workshop on Remote Sensing in Transportation. April 15, Madison, WI.

NCRST (2003c), Roadmap for Deploying UAVs in Transportation. December 2, Santa Barbara, CA.

NCRST (2004), Applications of Remote Sensing Technologies for Transportation Data Collection. December 1-2, Jacksonville, FL.

Poon, J., Fraser, C.S., Zhang, C., Zhang, L., & Gruen, A. (2005), Quality assessment of digital surface models generated from IKONOS imagery. *Photogrammetric Record*, 20(110):162-171.

Poon, J., Fraser, C.S., & Zhang, C. (2006), High-resolution satellite imaging for digital surface models. *International Archives of Photogrammetry and Remote Sensing*, 14-16 February, Ankara, Turkey. CDROM.

Puri, A., Valavanis, K. & Kontitsis, M. (2007), Generating traffic statistical profiles using unmanned helicopter-based video data, in *Proceedings of IEEE International Conference on Robotics and Automation*, 870-876.

Skorseth, K. & Selim, A. (2000), Gravel roads maintenance and design manual. Available at <http://www.epa.gov/owow/nps/gravelman.pdf>. Accessed on 20 July, 2007.

Sokolic, I., Gunaratne, M., Mraz, A. & Nazef, A. (2004), Evaluation of pavement distress imaging systems, in *Proceedings of 83rd Annual Meeting of the Transportation Research Board*. CDROM.

Srinivasan, S., Latchman, H., Shea, J., Wong, T. & McNair, J. (2004), Airborne Traffic Surveillance Systems – Video Surveillance of Highway Traffic, in *Proceedings of the ACM 2nd International Workshop on Video Surveillance & Sensor Networks*, 131-135.

Walker, D., Entine, L. & Kummer, S. (2002), Gravel PASER Manual, available on <http://tic.engr.wisc.edu>. Accessed on June 2007.

Wang, K.C.P. (2000), Design and implementation of automated systems for pavement surface distress survey, *ASCE Journal of Infrastructure System*, 6(1), 24-32.

Wang, K.C.P., Hou, Z., Watkins, Q.B. & Kuchikulla, S.R. (2007), Automated imaging technique for runway condition survey, in *Proceedings of 2007 FAA Worldwide Airport Technology Transfer Conference*, CDROM.

Xiang, H. & Tian, L. (2007), An autonomous helicopter system for aerial image collection, in *Proceedings of American Society of Agricultural and Biological Engineers Annual Meeting*. CDROM.

Zhang, C. (2003), Towards an operational system for automated updating of road databases by integration of imagery and geodata, *ISPRS Journal of Photogrammetry and Remote Sensing*, 58(3/4), 166-186.

Zhang, C. (2009), UAV-based Remote Sensing of Road Condition. Proc. of ASPRS Annual Conference. March 9 – 13, 2009, Baltimore, MD.

Zhang, C. & Elaksher, A. (2009), Photogrammetric Processing of Low-altitude UAV Imagery. Proc. of ASPRS Annual Conference. March 9 – 13, 2009, Baltimore, MD.

Zhang, C. & Fraser, C.S. (2008), Generation of digital surface model from high-resolution satellite imagery, *International Archives of Photogrammetry, Remote Sensing and Spatial Information Sciences*, Beijing, China. CDROM.

Zhang, Z.Y. (2000), A flexible new technique for camera calibration, *IEEE Transaction on Pattern Analysis and Machine Intelligence*, 22(11), 1330-34.

Zhou, G., Li, C. & Cheng, P. (2005), Unmanned aerial vehicle (UAV) real-time video registration for forest fire monitoring, in *Proceedings of the 2005 IEEE Geoscience and Remote Sensing Symposium*, Volume 3, 1803- 1806.

Appendix: List of Publications

Zhang, C., 2008. Development of a UAV-based Remote Sensing System for Unpaved Road Condition Assessment. Proc. of ASPRS Annual Conference. April 28 – May 2, Portland, OR.

Zhang, C., 2008. Development of a UAV-based Remote Sensing System for Unpaved Road Condition Assessment. International Achieve of Photogrammetry and Remote Sensing. July 3-13, Beijing, China.

Zhang, C., 2009. UAV-based Remote Sensing of Road Condition. Proc. of ASPRS Annual Conference. March 9 – 13, 2009, Baltimore, MD.

Zhang, C., Elaksher, A., 2009. Photogrammetric Processing of Low-altitude UAV Imagery. Proc. of ASPRS Annual Conference. March 9 – 13, 2009, Baltimore, MD.

Zhang, C., Elaksher, A., 2009. Development of an Unmanned Aerial Vehicle-Based Imaging System for 3D Measurement of Rural Road Surface Distresses. Computer-Aided Civil and Infrastructure Engineering. In review.

Zhang, C., 2010. Assessment of Rural Road Condition using UAV-based Remote Sensing. Proc. of Remote Sensing Technologies for Transportation Applications. January 10, Washington DC.